© 2020. Published by The Company of Biologists Ltd | Journal of Cell Science (2020) 133, jcs240077. doi:10.1242/jcs.240077

RESEARCH ARTICLE

Bosutinib prevents vascular leakage by reducing focal adhesion turnover and reinforcing junctional integrity

Liza Botros[1,2], Manon C. A. Pronk[2], Jenny Juschten[3], John Liddle[4], Sofia K. H. Morsing[5], Jaap D. van Buul[5], Robert H. Bates[4], Pieter R. Tuinman[3], Jan S. M. van Bezu[2], Stephan Huveneers[6], Harm Jan Bogaard[1], Victor W. M. van Hinsbergh[2], Peter L. Hordijk[2] and Jurjan Aman[1,*]

ABSTRACT

Endothelial barrier dysfunction leads to edema and vascular leak, causing high morbidity and mortality. Previously, Abl kinase inhibition has been shown to protect against vascular leak. Using the distinct inhibitory profiles of clinically available Abl kinase inhibitors, we aimed to provide a mechanistic basis for novel treatment strategies against vascular leakage syndromes. We found that the inhibitor bosutinib most potently protected against inflammation-induced endothelial barrier disruption. *In vivo*, bosutinib prevented lipopolysaccharide (LPS)-induced alveolar protein extravasation in an acute lung injury mice model. Mechanistically, mitogen-activated protein 4 kinase 4 (MAP4K4) was identified as important novel mediator of endothelial permeability, which signaled via ezrin, radixin and moesin proteins to increase turnover of integrin-based focal adhesions. The combined inhibition of MAP4K4 and Abl-related gene (Arg, also known as ABL2) by bosutinib preserved adherens junction integrity and reduced turnover of focal adhesions, which synergistically act to stabilize the endothelial barrier during inflammation. We conclude that MAP4K4 is an important regulator of endothelial barrier integrity, increasing focal adhesion turnover and disruption of cell–cell junctions during inflammation. Because it inhibits both Arg and MAP4K4, use of the clinically available drug bosutinib might form a viable strategy against vascular leakage syndromes.

KEY WORDS: Endothelial barrier function, Vascular permeability, Focal adhesion, Tyrosine kinase inhibitors, Bosutinib, MAP4K4

INTRODUCTION

The vascular endothelium controls the transport of proteins and solutes from the blood to the tissues (Mehta and Malik, 2006; Komarova et al., 2017). Dysregulation of the endothelial barrier leads to capillary leakage and edema, as seen in pathological conditions such as acute respiratory distress syndrome (ARDS) and sepsis (Lee and Slutsky, 2010; Komarova et al., 2017). Inflammatory mediators open endothelial cell junctions, enhancing vascular permeability (Wessel et al., 2014). Despite increased understanding of endothelial barrier regulation at the molecular level (Filewod and Lee, 2019), only supportive care with oxygen supplementation and lung-protective ventilation are available, but do not target the underlying inflammation-induced structural defects in the endothelium (Lee and Slutsky, 2010; Matthay et al., 2019).

Adherens junctions (AJs) comprise transmembrane proteins that form dynamic interactions between adjacent cells and play an important role in maintaining the integrity of the vascular endothelial monolayer and in the regulation of its barrier function (Dejana and Giampietro, 2012; Gavard, 2013). The main AJ protein is vascular-endothelial (VE)-cadherin, a single span transmembrane, homotypic adhesion molecule that connects intracellularly to the cortical F-actin cytoskeleton (Dejana and Giampietro, 2012). In the presence of pro-inflammatory stimuli, intracellular signalling leads to phosphorylation, destabilization and internalization of VE-cadherin (Gavard, 2013). In parallel, activation of RhoGTPases induces acto-myosin based contraction, following the phosphorylation of myosin light chain 2 (MLC2), which leads to contractile stress fibres, exertion of force on the junctional complexes and finally retraction of the cell membrane (Mehta and Malik, 2006; Huveneers et al., 2012).

We have previously demonstrated that the Abl kinase inhibitor (AKI) imatinib reverses pulmonary edema (Aman et al., 2013) and protects against endothelial barrier disruption by inhibition of Abl-related gene (Arg, also known as ABL2) (Aman et al., 2012). The inhibition of Arg resulted both in enhanced cell–cell interactions and enhanced cell–matrix adhesion. Mechanistically, we showed that imatinib-mediated inhibition of Arg increased the activity of Rac1 and the stabilization of peripheral, β1-integrin-containing, focal adhesions (FAs). FAs are multi-protein structures that link the cytoskeleton to the extracellular matrix (ECM) (Hynes, 2002). Within FAs, integrins play a pivotal role both in cell–matrix adhesion and in bidirectional signaling across the plasma membrane (Shattil et al., 2010). Similar to what is found for cadherins, the intracellular domains of integrins are dynamically connected to the actin cytoskeleton through a large variety of adapter and signaling proteins. As a result, integrin stability and adhesive function is subject to regulation by signaling from within the cell (‘inside-out’ signaling). Conversely, integrins probe the extracellular environment where their adhesive interactions with the ECM trigger subsequent intracellular (‘outside-in’) signaling (Shattil et al., 2010; Hynes, 2002).

Integrins are essential for endothelial barrier stability, cell migration and proliferation (Shattil et al., 2010; Yamamoto et al., 2015; Song et al., 2017) and there is growing evidence for a role of FA and β1-integrins in blood vessel stability and barrier function

[1]Amsterdam UMC, Vrije Universiteit Amsterdam, Department of Pulmonology, Amsterdam Cardiovascular Sciences, 1081 BT Amsterdam, The Netherlands. [2]Amsterdam UMC, Vrije Universiteit Amsterdam, Department of Physiology, Amsterdam Cardiovascular Sciences, 1081 BT Amsterdam, The Netherlands. [3]Amsterdam UMC, University of Amsterdam, Department of Intensive Care, 1105 AZ Amsterdam, The Netherlands. [4]GlaxoSmithKline, Stevenage, Hertfordshire, SG1 2NY, UK. [5]Molecular Cell Biology Lab at Dept. Molecular Cellular Haemostasis, Sanquin Research and Landsteiner Laboratory, Amsterdam, The Netherlands. [6]Amsterdam UMC, University of Amsterdam, Department of Medical Biochemistry, Amsterdam Cardiovascular Sciences, 1105 AZ Amsterdam, The Netherlands.

*Author for correspondence (j.aman@amsterdamumc.nl)

L.B., 0000-0001-8048-0240; J.D.v.B., 0000-0003-0054-7949; J.A., 0000-0001-6211-1791

Handling Editor: Arnoud Sonnenberg
Received 2 October 2019; Accepted 11 March 2020

Journal of Cell Science (2020) 133, jcs240077. doi:10.1242/jcs.240077

(Pulous et al., 2019; Hakanpaa et al., 2018; Yamamoto et al., 2015). Integrin-containing FAs have been shown to stabilize and localize VE-cadherin at cell–cell junctions (Pulous et al., 2019; Yamamoto et al., 2015), although the underlying mechanism remains unclear. The involvement of integrins in endothelial barrier regulation is diverse, and is dependent on the availability of different integrin subtypes and their cellular distribution (Su et al., 2012, 2007; Hakanpaa et al., 2018).

Next-generation AKIs have been developed to treat imatinib-resistant forms of chronic myeloid leukemia (Khoury et al., 2012), and these show different kinase inhibition and safety profiles. We hypothesized that inhibition of a favorable combination of kinases (as provided by next-generation AKIs) could provide greater potential for the treatment of vascular leakage syndromes. In the current study, we made use of the distinct inhibitory profiles of clinically available AKIs to provide a mechanistic basis for novel treatment strategies against vascular leakage syndromes (Gover-Proaktor et al., 2018). We identified the clinically available AKI bosutinib as robust protector of vascular permeability both *in vitro* and *in vivo*, and that it exerts its protective effect through combined inhibition of Arg and mitogen-activated protein kinase 4 (MAP4K4).

RESULTS

Bosutinib provides full protection against thrombin-induced endothelial barrier disruption

Previously, we identified the kinase inhibitor imatinib as a compound that protects against agonist-induced loss of barrier function (Aman et al., 2012). In search for novel, more effective barrier-protecting compounds, we tested three generations of Abl-kinase inhibitors on endothelial barrier function in human umbilical vein endothelial cells (HUVECs) (Fig. 1A,B; Fig. S1A,B). In these studies, we challenged stable endothelial monolayers with the protease thrombin, which represents a well-established model for inflammation-induced loss of endothelial integrity. Similar to other G-protein-coupled receptor agonists, the loss of barrier function induced by thrombin is acute and reversible (Fig. S1B). Our screen showed that the synthetic quinolone derivate bosutinib demonstrated the strongest protection to thrombin-challenged loss of endothelial barrier function. This was observed both in macromolecule passage assays (Fig. 1A; Fig. S1A) and in transendothelial electrical resistance assays (Fig. 1B; Fig. S1B). Validation experiments further confirmed that bosutinib increased basal barrier function (Fig. S1C), and that bosutinib protected against thrombin- and histamine-induced endothelial barrier disruption (Fig. 1C,D; Fig. S1D) at an optimal concentration of 1 µM (Fig. S1E,F). Cell viability assays showed no cell toxicity at this concentration (Fig. S1G). Similar protective effects were observed in human pulmonary microvascular endothelial cells (PMVECs) (Fig. 1E) showing that barrier protection by bosutinib is neither agonist nor endothelial cell type specific. These experiments demonstrate a strong protective effect of bosutinib against inflammation-induced endothelial barrier loss.

Subsequent immunofluorescence studies showed that bosutinib in both PMVECs and HUVECs protected against thrombin-induced intercellular gap formation (Fig. 1F,G; Fig. S1H,I), and increased VE-cadherin intensity at cell–cell junctions (Fig. 1F,H; Fig. S1H,J). Moreover, bosutinib increased the number of β1-integrin-positive FAs (Fig. 1F,I; Fig. S1H,K). Bosutinib did not reduce F-actin stress fiber formation or Ser18/Thr19-phosphorylation of MLC2 (Fig. S1L), indicating that bosutinib does not inhibit actomyosin contractility. Total VE-cadherin and vinculin levels did not change after bosutinib treatment, as shown in western blot assays (Fig. S1M,N). These results suggest that bosutinib protects against endothelial barrier disruption by enhancing VE-cadherin-containing adherens junctions and reinforcing β1-integrin-containing FAs.

Inhibition of MAP4K4 by bosutinib stabilizes endothelial barrier function

Our previous studies showed that imatinib prevents endothelial barrier dysfunction and edema via inhibition of Arg (Aman et al., 2012). As bosutinib had stronger barrier-protective effects than imatinib (Fig. 1A,B), we hypothesized that combined inhibition of multiple kinases favors endothelial barrier preservation under inflammatory conditions. To understand which kinases could be involved, bosutinib and imatinib were profiled by measuring the inhibitory activity against 369 kinases at a single concentration in competition binding assays. Thresholds for kinase inhibition of ≥75% at 10 nM bosutinib and ≤50% at 10 µM imatinib were chosen to select candidate kinases that might account for the differential effects of these two inhibitors on endothelial barrier function (Fig. 2A). Interestingly, bosutinib showed specificity against several mitogen-activated protein family kinases [MAP4K4, MAP4K5, MAP4K6 (also known as MINK1) and MAP4K7 (also known as TNIK)]. Since bosutinib showed highest specific kinase inhibition against MAP4K5, electric cell–substrate impedance sensing (ECIS) assays were used to compare barrier function between cells with siRNA-mediated knockdown of MAP4K5 (siMAP4K5) and those with knockdown of MAP4K4 (siMAP4K4), a kinase known to regulate focal adhesion and barrier function (Yue et al., 2014; Vitorino et al., 2015; Roth Flach et al., 2015). siRNA-mediated knockdown of MAP4K4 resulted in specific and efficient (>80%) depletion of MAP4K4 (Fig. S2A,B). To our surprise, depletion of MAP4K4, but not MAP4K5, significantly attenuated thrombin-induced barrier disruption (Fig. 2B; Fig. S2C). Simultaneous knockdown of both MAP4K4 and MAP4K5 did not further improve barrier protection (Fig. 2B,C). Different siRNAs for MAP4K4 displayed a similar degree of protective effect during thrombin stimulation (Fig. S2D).

As prolonged knockdown may result in compensatory upregulation of redundant pathways, we evaluated the effect of a pharmacological MAP4K4 inhibitor (PF-6260933) that inhibits the trio of MAP4K4, MAP4K6 and MAP4K7 (denoted MAP4K4/6/7) (Ammirati et al., 2015; Roth Flach et al., 2015). Treatment with PF-6260933 increased basal monolayer resistance and significantly attenuated the thrombin-induced loss of barrier function (Fig. 2C). MAP4K4 shares greater than 90% amino acid identity with MAP4K6 and MAP4K7 (Chuang et al., 2016), and redundancy and overlapping functions have been described for these kinases (Baumgartner et al., 2006; Chuang et al., 2016). Knockdown of MAP4K6 and MAP4K7 did not improve endothelial barrier function and combined knockdown of the trio MAP4K4/6/7 gave similar results compared to knockdown of MAP4K4 alone (Fig. 2D; Fig. S2E). Knockdown efficiency and specificity is depicted in Fig. S2A,F–H, showing that MAP4K5 had some cross-reactivity with MAP4K6 and MAP4K7.

As Arg is inhibited by both bosutinib and imatinib, we hypothesized that combined inhibition of Arg and MAP4K family of kinases, results in a similar protective effect as bosutinib treatment. To test this, macromolecule passage was measured under basal conditions, showing significant reduction of macromolecule passage in siMAP4K4 (Fig. S2I), in line with the

Journal of Cell Science (2020) 133, jcs240077. doi:10.1242/jcs.240077

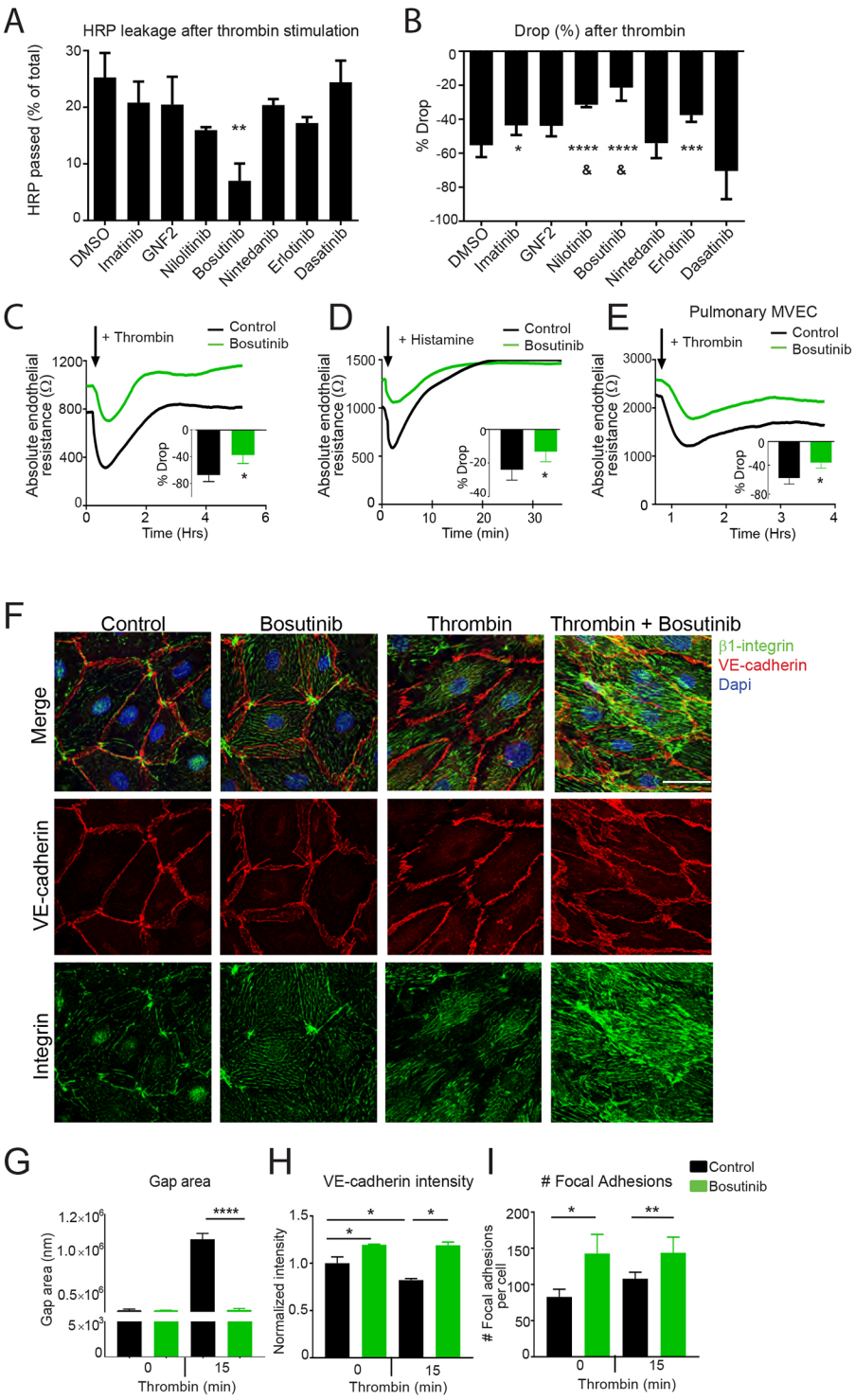

Fig. 1. Bosutinib provides robust protection against inflammation-induced endothelial barrier dysfunction. (A) Macromolecule passage over HUVEC monolayers after 2 h of thrombin stimulation with second- and third-generation tyrosine kinase inhibitors in their optimal concentration (n=5–6). Imatinib, 10 µM; GNF2, 10 µM; Nilotinib, 10 µM; Bosutinib, 1 µM; Nintedanib, 1 µM; Erlotinib, 10 µM; Dasatinib, 0.1 µM. (B) Quantification of the thrombin response as determined by calculating the maximal drop in endothelial resistance (%) as measured by ECIS. *P<0.05, **P<0.01, ***P<0.001, ****P<0.0001 compared to DMSO control and $^{\&}P$<0.05 compared to imatinib (n=6–8). (C,D) Absolute endothelial resistance in HUVECs and quantification of the thrombin and histamine response as determined by calculating the maximal drop in resistance (%) (n=3–4). (E) Absolute endothelial resistance in PMVECs and quantification of the thrombin response as determined by calculating the maximal drop in resistance (%) (n=3). (F) Immunofluorescence staining of active integrin β1 (green) and VE-cadherin (red) in control versus bosutinib-treated PMVECs counterstained with DAPI (blue). Scale bar: 50 µm. Representative images of n=3 experiments. (G) Gap area in control versus bosutinib treated PMVECs after 15 min of thrombin stimulation (n=3). (H,I) VE-cadherin intensity (membrane:cytosol ratio) and number of integrin β1-containing FAs in control versus bosutinib-treated PMVECs stimulated with thrombin (n=3). *P<0.05, **P<0.01, ****P<0.0001. All data is represented as mean±s.d. Comparison of two conditions was tested by Student's t-test (C,D,E). Comparison of more than two conditions was tested by one-way ANOVA (A,B,G,H,I).

barrier stabilizing effect of bosutinib (Fig. 1C). Knockdown of MAP4K4 either alone or combined with the loss of Arg effectively reduced thrombin-induced macromolecule passage, although this effect did not mimic the protective effect of bosutinib completely (Fig. S2J). Likely, acute kinase inhibition with bosutinib is more effective in barrier protection as compared to the siRNA-mediated loss of cognate kinase expression quantified only after 72 h. Knockdown of Arg combined with PF-6260933 completely mimicked the positive effect of bosutinib on basal endothelial barrier function as well as thrombin-induced loss of integrity (Fig. 2D; Fig. S2K,I). Taken together, these data show that combined kinase inhibition of Arg and MAP4K4 can account for the protective effects of bosutinib on endothelial barrier function.

To evaluate the effect of MAP4K4 on cell–cell junctions and cell–ECM interaction, immunostaining for VE-cadherin, active β1-integrin and F-actin was performed after treatment with siMAP4K4, siArg and PF-6260933 (Fig. 3A). VE-cadherin intensity was unaltered under basal conditions (Fig. S3A,B). After thrombin stimulation, MAP4K4 knockdown or its inhibition completely prevented intercellular gap formation (Fig. 3A,B). In line with this, thrombin-induced loss of

Journal of Cell Science

Journal of Cell Science (2020) 133, jcs240077. doi:10.1242/jcs.240077

A

	Average inhibition	
Kinase	Bosutinib	Imatinib
ABL2/ARG	99.7	95.3
KHS/MAP4K5	99.4	10.3
PEAK1	98.9	21.1
C-SRC	98.5	24.7
FRK-PTK5	96.0	39.2
YES	94.8	63.7
FYN	89.1	66.8
EPHB4	86.5	23.0
EPHB2	84.9	28.1
TNIK/ MAP4K7	84.7	66.0
BTK	83.8	16.9
NTRK3	83.7	59.5
SIK2	83.1	9.0
EPHB1	82.5	30.6
EPHA4	81.6	26.7
EPHA2	80.6	51.0
CSK	80.1	34.9
SIK1	78.0	9.6
MINK1 / MAP4K6	77.8	51.7
HGK / MAP4K4	75.0	41.4

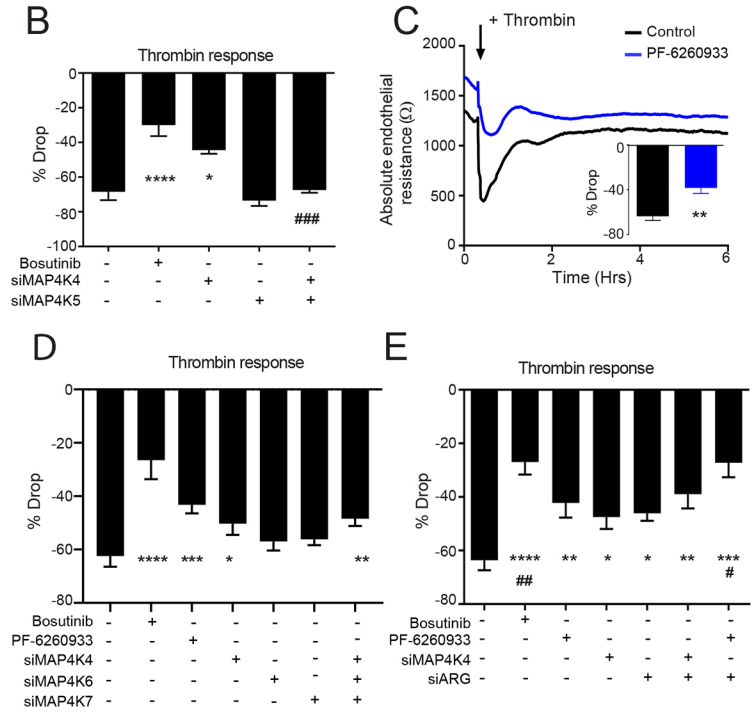

Fig. 2. Inhibition of MAP4K4 by bosutinib enhances endothelial barrier function. (A) Comparison of the kinase inhibitory activity of the Abl tyrosine kinase inhibitors bosutinib and imatinib. At a threshold of ≥75% inhibition at 10 nM bosutinib and ≤50% at 10 µM imatinib, 13 kinases were identified to be inhibited by 1 µM bosutinib but not by 10 µM imatinib (shown in green), including the MAP4K family of kinases (MAP4K4, MAP4K5, MAP4K6 and MAP4K7). (B) Quantification of the thrombin response as determined by calculating the maximal drop in resistance after siMAP4K4 and siMAP4K5 (%) (n=3–5). (C) Absolute endothelial resistance of HUVEC monolayers and percentage drop during thrombin stimulation with 3 µM of the pharmacological MAP4K4 inhibitor PF-6260933 (n=3). (D) Quantification of the thrombin response as determined by calculating the maximal drop in resistance after bosutinib treatment, PF-6260933 treatment and the knockdown of MAP4K4/6/7 (n=3). Quantification of the thrombin response as determined by calculating the maximal drop in resistance after knockdown and inhibition of MAP4K4 with knockdown of Arg (%) (n=5). *P<0.05, **P<0.01, ***P<0.001, ****P<0.0001 compared to NT control; $^{\#}P$<0.05, $^{\#\#}P$<0.01, $^{\#\#\#}P$<0.0001 compared to siMAP4K4. All data is represented as mean±s.d. Comparison of two conditions was tested by Student's t-test (C). Comparison of more than two conditions was tested by one-way ANOVA (B,D,E).

VE-cadherin intensity at the cell periphery was fully preserved after PF-6260933 treatment (Fig. 3C). Similar to what was seen with bosutinib treatment, the number of FAs increased after inhibition or loss of MAP4K4 under basal conditions (Fig. S3C) as well as in thrombin-stimulated cells (Fig. 3D). Peripheral focal adhesions were increased with bosutinib treatment, PF-6260933, siMAP4K4, and siArg with PF-6260933 (Fig. 3E). Since the total number of FAs also increased, the ratio remained unaltered in all conditions except bosutinib treatment (Fig. 3F).

In line with the effects of bosutinib on the F-actin cytoskeleton (Fig. S1H), stress fiber formation was not affected by the loss or inhibition of Arg or MAP4K4 (Fig. S3A), indicating that increased acto-myosin-based contraction is not sufficient for intercellular gap formation. Taken together, these data provide further evidence that MAP4K4 and Arg both negatively regulate the stabilization of FAs and adherens junctions, and that combined loss or inhibition of these kinases might recapitulate the strong barrier protective effects of bosutinib.

MAP4K4 increases FA turnover

As recent studies pointed to a role for β1-integrin activation in maintaining VE-cadherin at AJs (Yamamoto et al., 2015; Pulous et al., 2019; Hakanpaa et al., 2018) and bosutinib enhanced β1-integrin localization in peripheral FAs (see Figs 1F,I and 3D–F), we tested whether MAP4K4 inhibition may have an additional effect via FA reorganization. The involvement of MAP4K4 in FA dynamics was analyzed using live-cell imaging of primary human endothelial cells expressing GFP–vinculin (Movies 1–3). Time lapse images of GFP–vinculin-expressing endothelial cells show basal FA dynamics after treatment with bosutinib or PF-6260933, followed by thrombin stimulation. In line with the data in Fig. 3B, both bosutinib and PF-6260933 increased the abundance of FAs in unstimulated and in thrombin-treated cells (Fig. 4A). We next quantified FA turnover, which showed that FA assembly and disassembly were decreased by bosutinib and PF-6260933 under basal and thrombin-stimulated conditions (Fig. 4B,C). This results in increased FA lifetime (Fig. 4D). In further support of a FA-stabilizing effect, bosutinib increased cell spreading, as measured by ECIS (Fig. S3D,E) and by microscopy (Fig. 4E), without changing F-actin levels or MLC2 phosphorylation (Fig. S1L).

Because MAP4K4 inhibition induced stabilization of both FAs and AJs, we evaluated whether the observed FA stabilization contributes to AJ stabilization and endothelial barrier protection by bosutinib. We therefore used peptides that block integrin adhesive function (GRGDSP and GRGDNP) to evaluate whether bosutinib still protects the endothelial barrier in the absence of functional integrins and FAs. GRGDSP is described to bind αvβ5 and α5β1 but with preferential binding to αvβ3; GRGDNP also blocks adhesion by αvβ3 and α5β1 with similar specificity but preferential binding to α5β1 (Kapp et al., 2017). As measured by transendothelial resistance, the simultaneous addition of GRGDSP and/or GRGDNP induced a loss of endothelial integrity in a concentration-dependent manner (Fig. S3F). No

Journal of Cell Science (2020) 133, jcs240077. doi:10.1242/jcs.240077

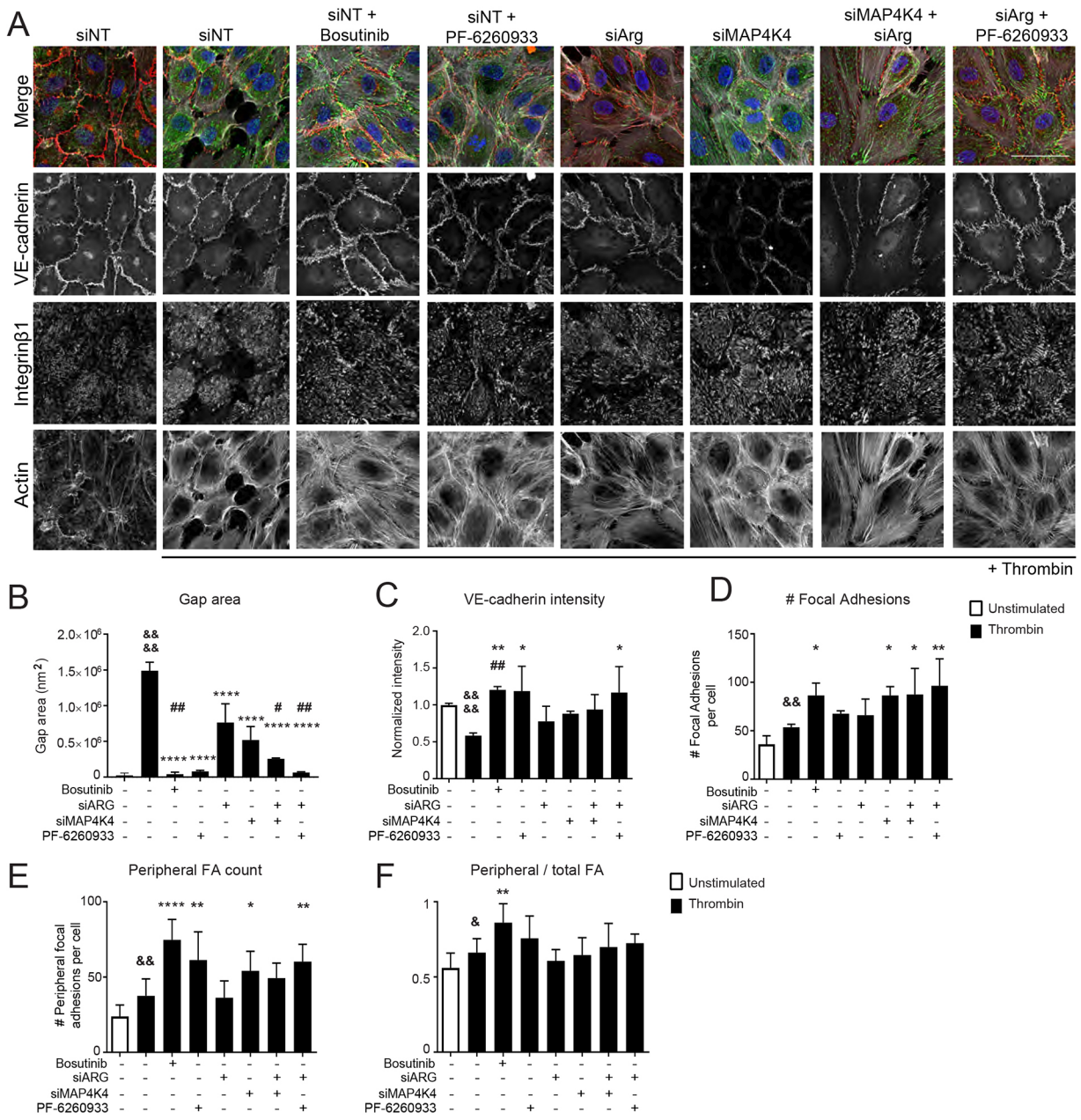

Fig. 3. MAP4K4 inhibition increases endothelial barrier integrity. (A) Immunofluorescence stainings of active integrin β1 (green), actin (white) and VE-cadherin (red) under basal and thrombin-stimulated conditions and counterstained with DAPI (blue). Results after treatment with bosutinib were compared with those after treatment with PF-6260933, siMAP4K4 and siArg. Scale bar: 50 µm. Representative images of *n*=4 experiments. (B) Quantification of the gap area after 15 min of thrombin stimulation (*n*=3). (C) Quantification of VE-cadherin intensity at the membrane divided by the intensity in the cytosol (*n*=3). (D) Quantification of FA count as determined by active integrin β1 staining (*n*=3). (E) Quantification of peripheral FA count per cell and (F) ratio of peripheral:total FA. **P*<0.05, ***P*<0.01, *****P*<0.0001 compared to the thrombin response; $^{\&}P$<0.05, $^{\&\&}P$<0.01, $^{\&\&\&\&}P$<0.0001 for the thrombin response compared to basal conditions; $^{\#}P$<0.05, $^{\#\#}P$<0.01 compared to siMAP4K4. All data is represented as mean±s.d. Comparison of two conditions was tested by Student's *t*-test (thrombin response B–F). Comparison of more than two conditions was tested by one-way ANOVA (B–F).

differences were observed between the different peptides when tested individually (Fig. S3G,H). When using integrin-β1-blocking peptides in a low concentration at which the basal barrier function was not compromised (450 µM), we found that bosutinib no longer rescued the thrombin-induced drop in barrier function (Fig. 4F,G; Fig. S3I). These results indicate that functional integrins are required for the barrier-protective effects of bosutinib and that they help to stabilize the endothelial barrier during thrombin-induced actomyosin contraction.

The MAP4K4–ERM pathway drives FA turnover during endothelial barrier disruption

Since MAP4K4 enhances FA turnover via phosphorylation of the ezrin, radixin and moesin (ERM) group of proteins (Vitorino et al., 2015), and since MAP4K4 directly binds the N-terminus of moesin (Baumgartner et al., 2006), we hypothesized that MAP4K4 signals via ERM proteins to stabilize FAs and barrier function. In immunofluorescence studies, siMAP4K4 or PF-6260933 reduced junctional localization and intensity of phosphorylated ERM (Fig. 5A,B). Moreover, bosutinib treatment significantly

Journal of Cell Science (2020) 133, jcs240077. doi:10.1242/jcs.240077

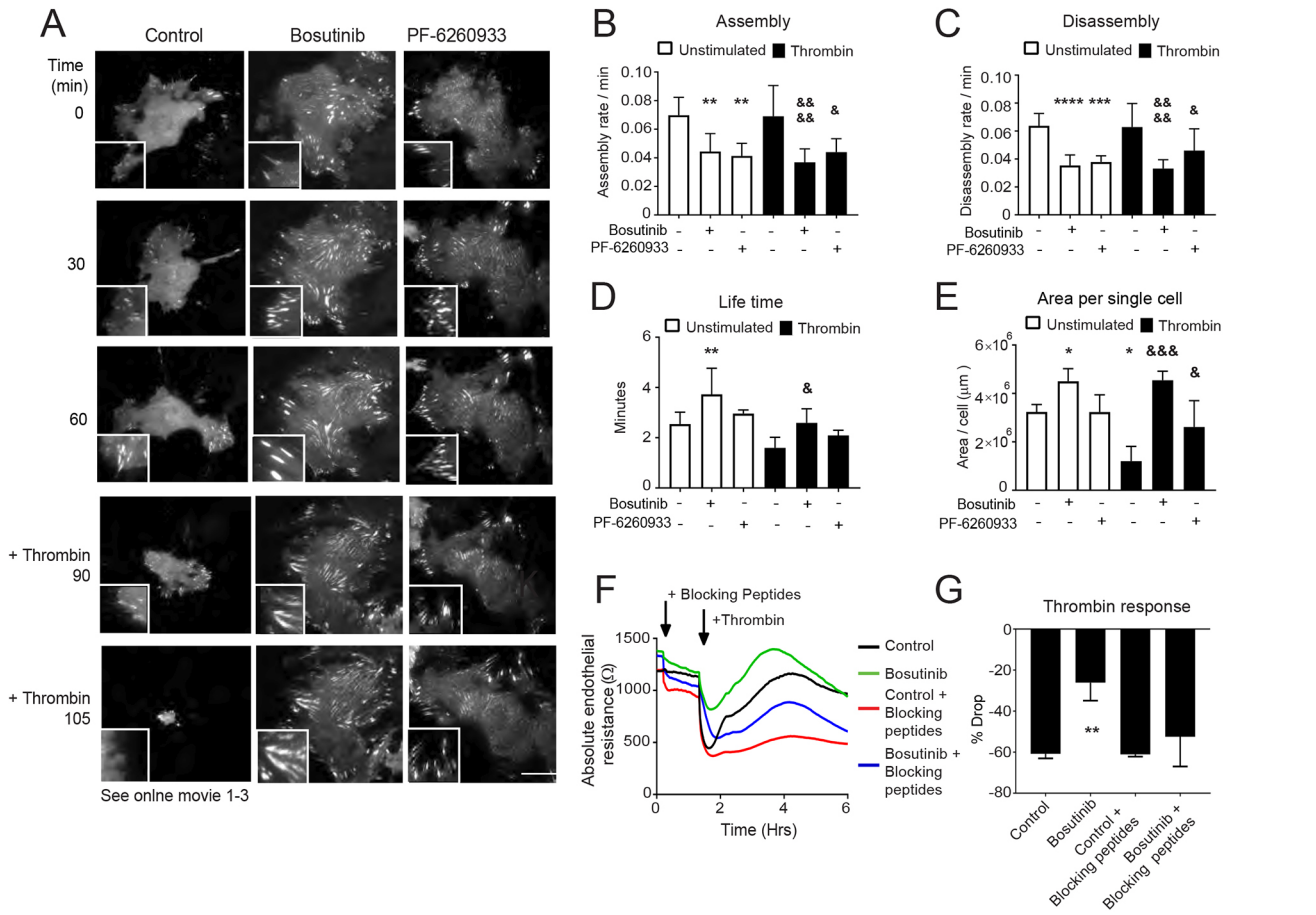

Fig. 4. MAP4K4 enhances FA turnover. (A) Representative images of movies on vinculin-containing FA imaged by TIRF microscopy every 30 s in control (DMSO), or after bosutinib or PF-6260933 treatment. Thrombin was added after 90 min. Scale bar: 50 µm. (B–D) Live-cell imaging analysis of single adhesions, including assembly rate (B), disassembly rate (C) and longevity (D) of GFP–vinculin under control (1 h imaging) and thrombin-stimulated (30–45 min imaging) conditions with bosutinib or PF-6260933 treatment (n=9–16 positions in two experiments). (E) Quantification of single-cell area after treatment with bosutinib and PF-6260933 under basal conditions and after 90–105 min of thrombin stimulation. (F) Absolute endothelial resistance of HUVEC monolayers with thrombin stimulation. Control (black), bosutinib treatment (green), control with addition of 450 µM peptides that block the adhesive function of integrins αvβ5, α5β1 and αvβ3 (red) and bosutinib treatment with addition of 450 µM peptides that block the adhesive function of integrins αvβ5, α5β1 and αvβ3 (blue) (n=3). (G) Quantification of maximal drop in resistance (%) after treatment with αvβ5, α5β1 and αvβ3 integrin-blocking peptides (n=3) *P<0.05, **P<0.01, ***P<0.001, ****P<0.0001 compared to control; $^{\&}P$<0.05, $^{\&\&\&}P$<0.01, $^{\&\&\&\&}P$<0.001 compared to thrombin stimulation. All data is represented as mean±s.d. Conditions were tested by one-way ANOVA (B–G).

decreased total phosphorylation of ERM proteins, as determined by western blotting, upon thrombin stimulation at several time points (Fig. 5C). This was not seen in cells treated with siMAP4K4, siArg or PF-6260933 (Fig. 5D; Fig. S4A).

To test whether ERM proteins act downstream of MAP4K4 during thrombin-induced barrier disruption, we compared the effect of silencing ezrin and moesin (siEzrin+siMoesin), both expressed in endothelial cells (Adyshev et al., 2013) with loss of MAP4K4 on thrombin-induced barrier disruption (see Fig. S4B for knockdown efficiency). Although siMAP4K4 and siEzrin+siMoesin attenuated the thrombin-induced drop in endothelial barrier function to a similar extent, combined siEzrin+siMoesin and siMAP4K4 had an additive protective effect (Fig. 5E; Fig. S4C). This can be explained by the fact that we observed restoration of VE-cadherin junctional intensity after thrombin stimulation in siEzrin+siMoesin-treated cells, but not in siMAP4K4-treated cells (Fig. 5F,G). Furthermore, siMAP4K4 and siEzrin+siMoesin increased the number of FAs to a similar extent, whereas the triple knockdown had no additive effect (Fig. 5H). Taken together, these data indicate that ERM proteins act downstream of MAP4K4 in stabilization of β1-integrin-based FAs, whereas ERM proteins stabilize junctional VE-cadherin in a MAP4K4-independent manner.

Bosutinib treatment attenuates LPS-induced pulmonary vascular leakage

Bosutinib is currently in clinical use for the treatment of chronic myeloid leukemia (Khoury et al., 2012; Kong et al., 2017). Repurposing bosutinib for prevention of vascular damage and edema would have large clinical benefit. We therefore tested the vascular barrier protective effects of bosutinib in a clinically relevant mouse model for pulmonary vascular leakage. Lung inflammation and edema were induced via intranasal administration of lipopolysaccharide (LPS) in mice concomitantly treated with bosutinib (20 mg/kg of body weight) or saline (control) injection as previously described (Tuinman et al., 2013) (Fig. 6A). Lung vascular leakage, measured by the lung weight to body weight ratio and protein concentration in bronchoalveolar lavage fluid (BALF), was significantly increased in the LPS-treated animals and this effect was prevented by bosutinib (Fig. 6B,C). As an additional measure of vascular leakage, 0.5% Evans Blue was administered

Journal of Cell Science (2020) 133, jcs240077. doi:10.1242/jcs.240077

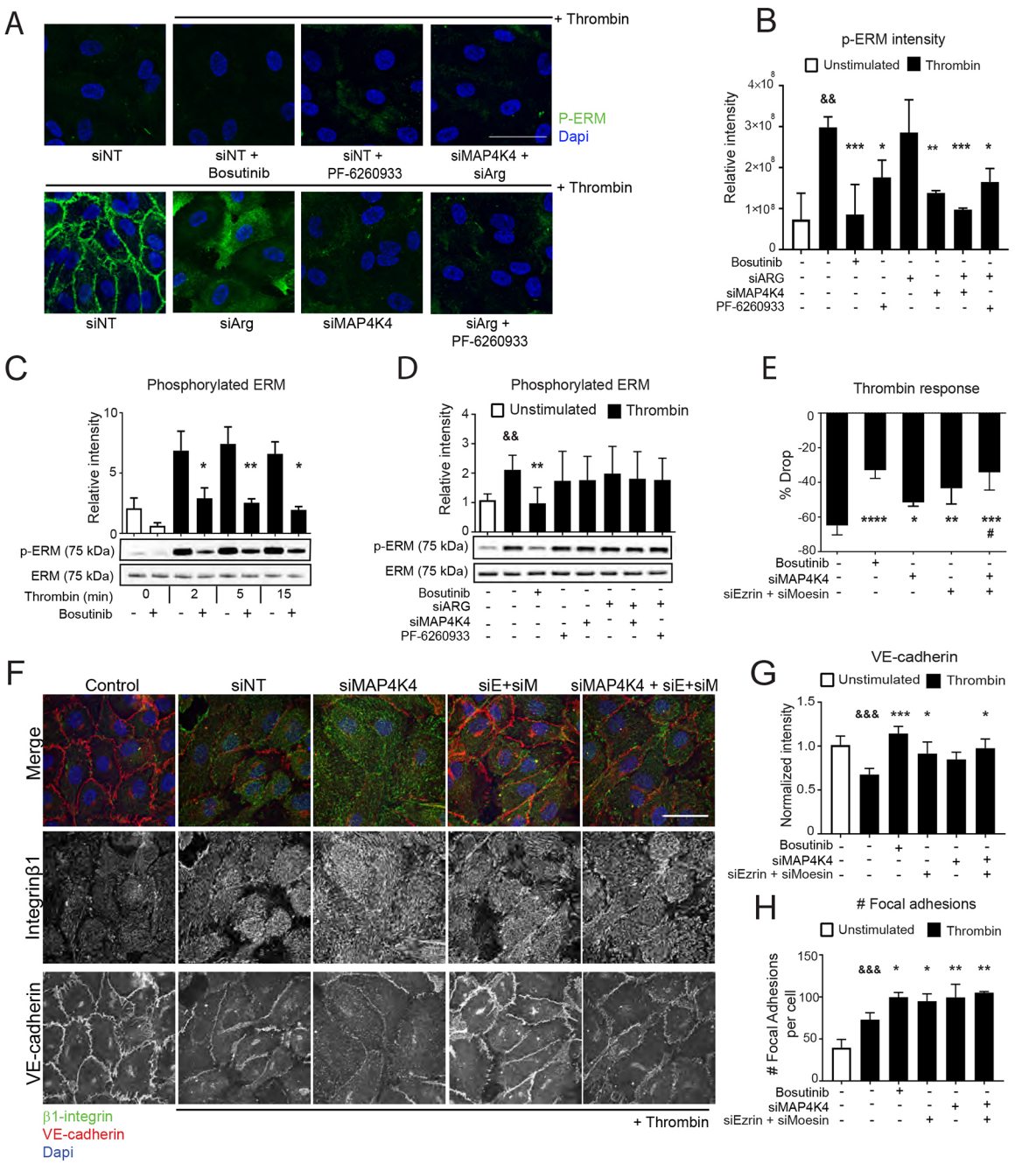

Fig. 5. The MAP4K4-ERM pathway drives FA turnover during endothelial barrier disruption. (A) Phospho ezrin (Thr567)/radixin (Thr564)/moesin (Thr558) (P-ERM, green) counterstained with DAPI (blue) in basal conditions and with 5 min of thrombin stimulation in siNT, siNT+bosutinib, siNT+PF-6260933, siARG, siMAP4K4 and siARG+siMAP4K4 or siArg+PF-6260933 (representative images of n=3) conditions. Scale bar: 50 µm. (B) Quantification of P-ERM intensity in immunofluorescence stainings (n=3). (C) Western blot analysis of P-ERM levels after thrombin stimulation at 0, 2, 5 and 15 min compared to total ERM levels (n=3). (D) Western blot analysis of P-ERM levels after thrombin stimulation for 5 min compared to total ERM levels (n=3). (E) Quantification of maximal drop in resistance in ECIS (%) after thrombin with bosutinib, siMAP4K4 and siEzrin+siMoesin (n=3–4). (F) Immunofluorescence staining for active integrin β1 (green) and VE-cadherin (red), and counterstained with DAPI (blue) under basal conditions and with thrombin stimulation for 15 min in siNT, siMAP4K4, siEzrin plus siMoesin (siE+siM), and the combination. Representative images of n=4 experiments. Scale bar: 50 µm. (G) Quantification of VE-cadherin intensity (membrane: cytosol ratio) after 15 min of thrombin stimulation (n=3–5). (H) Quantification of FA number after 15 min of thrombin stimulation (n=4–5). *P<0.05, **P<0.01, ***P<0.001, ****P<0.0001 compared to control; $^{\&\&}P$<0.01, $^{\&\&\&}P$<0.001 thrombin response compared to unstimulated condition; $^{\#}P$<0.05 compared to siMAP4K4. All data is represented as mean±s.d. Comparison of two conditions was tested by Student's t-test (thrombin response in B,C,D,G,H). Comparison of more than two conditions was tested by one-way ANOVA (B,C,D,E,G,H).

intravenously 5 h after the induction of lung injury, and organs were harvested 1 h after Evans Blue administration. Evans Blue extravasation was significantly increased in lungs and kidneys of LPS-treated mice, an effect that was prevented in bosutinib-treated mice (Fig. S5A–C).

Inflammation, measured by total cell count, percentage neutrophils together with IL-6 levels in BALF were markedly increased after LPS administration and significantly attenuated by bosutinib treatment (Fig. 6D–F), although active trans-endothelial neutrophil migration over pulmonary endothelial cells was not

Journal of Cell Science (2020) 133, jcs240077. doi:10.1242/jcs.240077

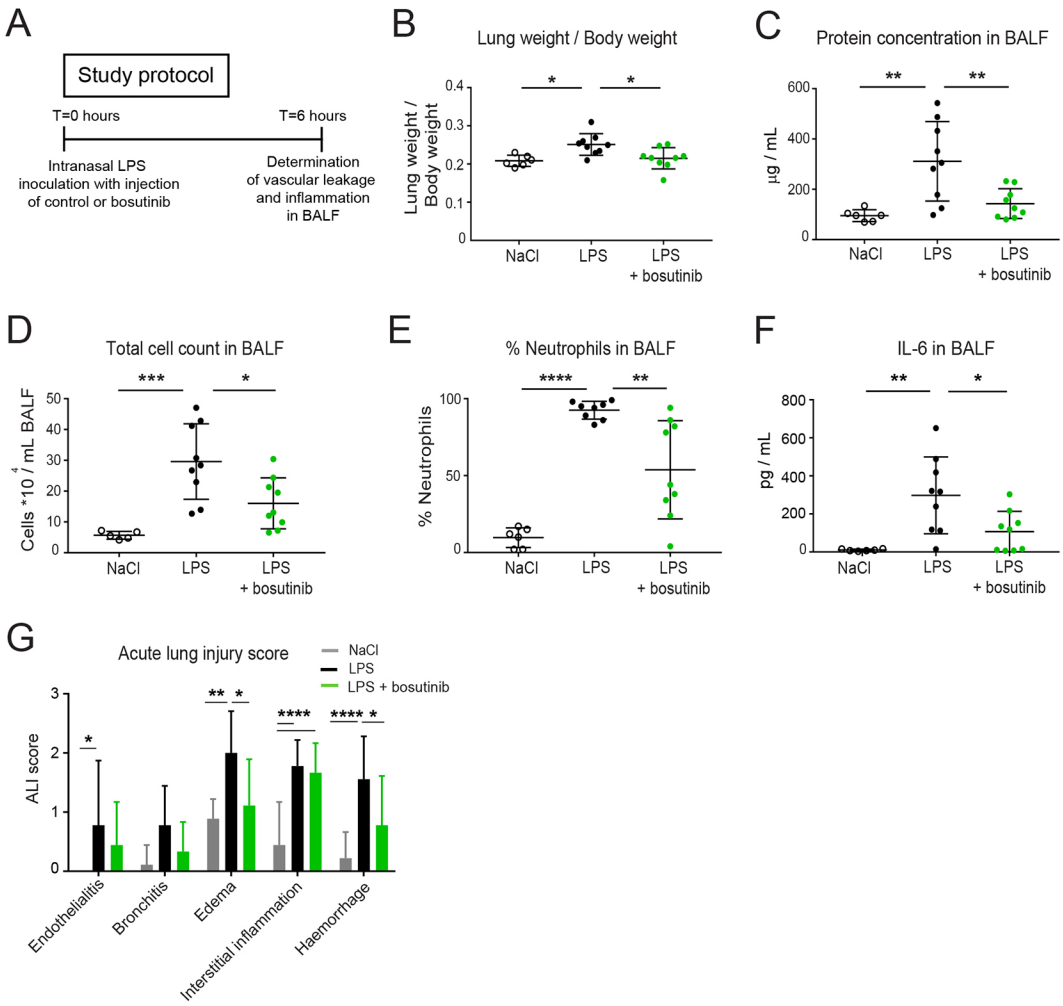

Fig. 6. Bosutinib treatment attenuates LPS-induced pulmonary vascular leakage. (A) Lung injury was induced in 42 male C57/BL6J mice by intranasal inoculation of LPS to assess the effect of bosutinib on direct LPS-induced lung injury. (B,C) Vascular leakage was determined by calculating the ratio of lung weight divided by the body weight, and by measuring protein concentration in BALF (n=6–9 per group). (D–F) Inflammation in BALF as determined by measuring the total cell count, percentage neutrophils and IL-6 concentrations in BALF (n=6–9 per group). (G) Acute lung injury score quantified blind in histological coupes of right lungs (n=6–9 per group). *P<0.05, **P<0.01, ***P<0.001, ****P<0.0001. All data is represented as mean±s.d. Conditions were tested by one-way ANOVA (B–G).

affected by bosutinib (Fig. S5F). TNF-α concentration in BALF was increased after LPS exposure, however, no significant reduction was observed with bosutinib treatment (Fig. S5D). A systemic inflammatory cytokine response, as measured by determining the circulating IL-6 levels in plasma, was not observed (Fig. S5E). As an additional measure of direct lung injury, the LPS-treated mice showed a significantly higher histopathology score in endothelialitis, edema, interstitial inflammation and hemorrhage in the lungs, whereas bosutinib significantly reduced edema and hemorrhage scores (Fig. 6G). These data demonstrate that repurposing the clinically available drug bosutinib effectively reduces inflammation-induced lung vascular leakage.

DISCUSSION

While the molecular basis of endothelial integrity has been extensively studied, compounds that provide effective protection against vascular leak, strongly associated with inflammatory disease, remain to be identified. Here, we show that the AKI bosutinib provides full protection against agonist-induced endothelial and vascular permeability *in vitro* and *in vivo*. We identified MAP4K4 as an important regulator of endothelial barrier function, contributing to adherens junction dissociation and signaling via ERM to increase FA turnover, with subsequent cell retraction and barrier disruption (Fig. 7). Our data support a model in which the turnover of peripheral, β1-integrin containing FAs contributes to the loss of VE-cadherin-mediated cell–cell contact (Fig. 7) (Pulous et al., 2019; Pulous and Petrich, 2019). While we previously showed that the first generation AKI imatinib provides partial protection from vascular leak by inhibiting Arg, bosutinib is more effective due to its additional effect on MAP4K4, a kinase only moderately targeted by imatinib (Fig. 2A).

Identification of MAP4K4 as regulator of endothelial barrier function

The regulation and function of individual serine/threonine MAP4K family of kinases is largely unknown, although MAP4K4 has repeatedly emerged as regulator of cell migration, adhesion and FA stabilization (Yue et al., 2014; Huang et al., 2004; Tripolitsioti et al., 2018; Machida et al., 2004). MAP4K4 activation by TNFα (also known as TNF) regulates important inflammatory responses

Journal of Cell Science (2020) 133, jcs240077. doi:10.1242/jcs.240077

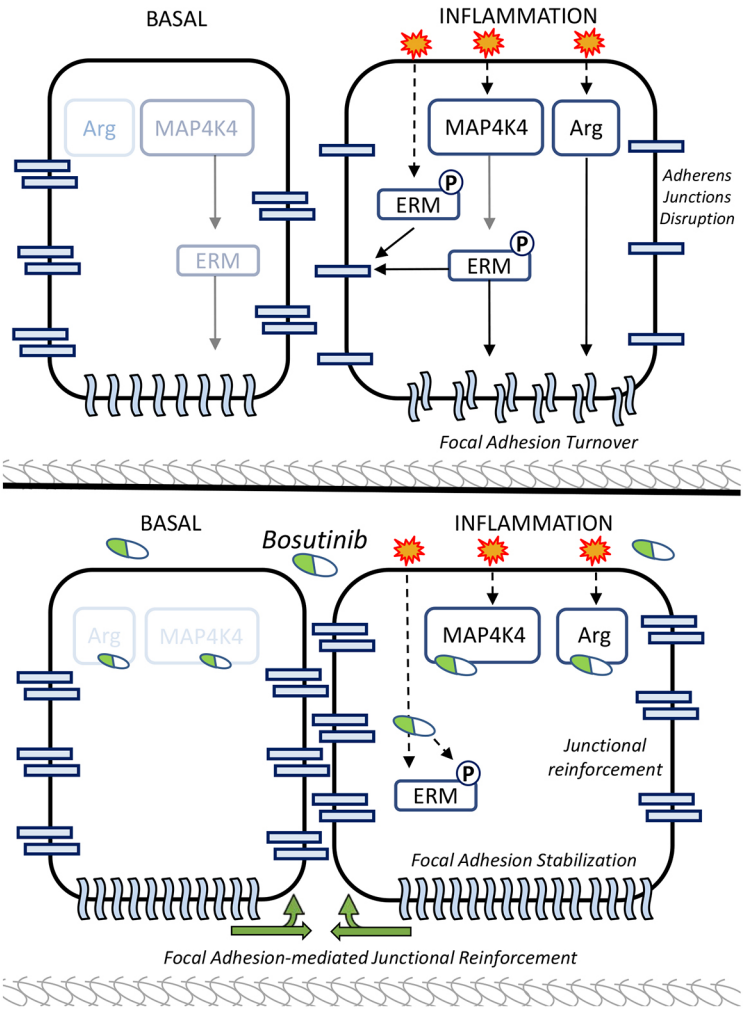

Fig. 7. Proposed mechanism of bosutinib and its barrier protective effects. (A) Under basal conditions, Arg is not active and minor MAP4K4 activity results in minimal FA turnover. During inflammation, for example in thrombin-stimulated conditions, MAP4K4 and Arg signal to increase FA turnover, reducing cell–matrix adhesion. MAP4K4 either phosphorylates a portion of the ERM proteins at a specific location in the cell and/or affects the translocation of phosphorylated ERM proteins as indicated by a gray arrow, disrupting AJs. (B) Bosutinib (indicated as the white–green tablet), inhibits several kinases including Arg and MAP4K4, enhancing basal barrier integrity. During inflammation, for example in thrombin-stimulated conditions, bosutinib prevents FA turnover through Arg and MAP4K4 inhibition. Bosutinib inhibits ERM activity directly, as well as through a MAP4K4-inhibiting effect. This results in junctional reinforcement and increased cell–cell contact. Stable FAs further signal to AJs, to increase endothelial barrier integrity.

including cytokine production as well as atherosclerosis and insulin resistance (Ammirati et al., 2015; Roth Flach et al., 2015; Huang et al., 2014). Divergent findings regarding a role for MAP4K4 in endothelial barrier function have been reported. Vitorino et al. found no role for MAP4K4 in basal endothelial permeability when using siRNA-mediated knockdown approach (Vitorino et al., 2015). On the other hand, others have reported that depletion of MAP4K4 increased basal barrier resistance (Pannekoek et al., 2013) and that macromolecule permeability was reduced in MAP4K4-silenced monolayers basally, and after TNFα-mediated inflammation *in vitro* (Roth Flach et al., 2015). A role for MAP4K4 for barrier function has been suggested by the observations that inhibition of MAP4K4 reduces cholesterol accumulation in aorta of mice and knockdown of MAP4K4 increased basal endothelial barrier function (Roth Flach et al., 2015; Pannekoek et al., 2013). The other members of the MAP4K serine/threonine kinase family, MAP4K6 and MAP4K7, share a common function in regulating cell shape and migration with MAP4K4, and these three kinases show greater than 90% amino acid identity (Baumgartner et al., 2006). Despite this structural similarity only knockdown of MAP4K4, but not MAP4K6 and MAP4K 7 protected against endothelial barrier disruption during inflammation.

The effect on FA distribution seen with bosutinib and MAP4K4 is mediated by ERM

We observed that bosutinib and MAP4K4 inhibition stabilized FA dynamics, leading to increased spreading of endothelial cells to the ECM. Since we found imatinib to increase predominantly peripheral FAs through Arg inhibition (Aman et al., 2012; Rizzo et al., 2015), we propose that bosutinib exerts an additional effect on FA dynamics by increasing β1 integrin and FA stability and longevity through MAP4K4 inhibition. Indeed, loss of MAP4K4 and moesin increased the number of both central and peripheral FAs (Vitorino et al., 2015). Moesin is the most abundant ERM protein in endothelial cells, and the individual ERM proteins show functional redundancy (Adyshev et al., 2013; Fehon et al., 2010). ERM proteins control cell shape through crosslinking the actin cytoskeleton to the plasma membrane (Tachibana et al., 2015; Baumgartner et al., 2006; Adyshev et al., 2013) and phosphorylation of ERM proteins after thrombin stimulation induces their translocation to the cell periphery, modulating AJ integrity and promoting gap formation (Adyshev et al., 2013; Amsellem et al., 2014). Phosphorylated ERM proteins were previously also detected in endothelial retraction fibers, linking ERM phosphorylation to the induction of contraction (Vitorino et al., 2015). In line with these observations, the present study demonstrates that ERM proteins act downstream of MAP4K4 to regulate β1 integrin activity and FA turnover during inflammation. As MAP4K4 inhibition increased cell adhesion and spreading, the MAP4K4/ERM pathway appears as an important mediator of decreased cell–ECM binding of endothelial cells under inflammatory conditions, although we cannot exclude a role for ERM protein in endothelial barrier regulation independent from MAP4K4.

Journal of Cell Science (2020) 133, jcs240077. doi:10.1242/jcs.240077

Interaction between FAs and AJs in endothelial barrier regulation

The protective effects of bosutinib were paralleled by improvement of AJ integrity and FA stability. Whereas the contribution of the AJ to endothelial barrier integrity is undisputed, the functional role of FA, and specifically integrins, is more controversial. We showed that peptides blocking the adhesive function of integrins αvβ5, α5β1 and αvβ3 counteracted the protective effect of bosutinib, indicating that FAs are functionally involved in endothelial barrier regulation and required for a functional barrier. It is known that β1-integrin interacts directly with talin (Giancotti, 2000) and that β1-integrins stabilize cell–cell contacts (Yamamoto et al., 2015; Pulous et al., 2019; Song et al., 2017). Although it is reported that integrin engagement leads to disruption of VE-cadherin containing AJs via the activation of Src kinase (Wang et al., 2006) and that β1-integrin-inhibiting antibodies decrease LPS-induced vascular leakage in murine endotoxemia (Hakanpaa et al., 2018), our data demonstrate that bosutinib decreases FA turnover and enhances cell adhesion to impair cell retraction, even in the presence of intact acto-myosin contraction. Although previous studies have shown that intact FAs are essential for a mature endothelial barrier (Song et al., 2017; Pulous et al., 2019; Yamamoto et al., 2015) the present study is the first to demonstrate that active regulation of FA turnover contributes to the hyperpermeability response *in vitro* and *in vivo*. Inhibition of Arg and MAP4K4 simultaneously with ERM-mediated reinforcement of the AJ, leads to barrier stabilization. This mechanism aligns well with the suggestion in previous studies that peripheral FA reinforce AJ integrity (Hakanpaa et al., 2018; Pulous et al., 2019).

Perspective

Bosutinib attenuated vascular leakage, protein extravasation and inflammation in a murine acute lung injury model, in line with previous research on virus-induced vascular leakage in human pulmonary endothelial cells (Gorbunova et al., 2011) and recovery of lung inflammation in an animal model for silicosis (Carneiro et al., 2017). In addition, in our study LPS and bosutinib were administered simultaneously preventing the development of lung edema. Active neutrophil migration remained unchanged *in vitro*, therefore we could not exclude a direct effect of bosutinib on neutrophil migration. As a clinically available drug, bosutinib is orally administered and well tolerated (Cortes et al., 2018), with milder cardiac hypertrophy and fewer vascular adverse events compared to several other AKIs (Heyen et al., 2013; Gover-Proaktor et al., 2018). Moreover, only low-grade gastrointestinal toxicity is reported after bosutinib treatment (Kong et al., 2017). Based on these drug characteristics, the fact that bosutinib inhibits endothelial MAP4K4 during inflammation, and the protective effects of bosutinib on vascular endothelial integrity identified in this study, repurposing bosutinib as novel treatment for clinical syndromes associated with vascular leak is a suitable option.

Conclusion

During inflammation, Arg and MAP4K4 signal to increase turnover of integrin-based peripheral FAs, which is required for the loss of VE-cadherin mediated cell-cell contact. This study identifies MAP4K4/ERM signaling as important pathway that mediates stimulus induced FA dissolution and adherens junction dissociation. Since the clinically available drug bosutinib inhibits both Arg and MAP4K4/ERM signaling, bosutinib may be a viable strategy against vascular leakage.

MATERIALS AND METHODS

Reagents, antibodies and siRNAs

For all experiments bosutinib was purchased from Selleck chemicals (s104) and dissolved in DMSO in a concentration of 1 µM. Imatinib (free base) was purchased from ChemieTek (Indianapolis, IN) and dissolved in DMSO in a concentration of 10 µM. All tyrosine kinases used in the screen were provided by GlaxoSmithKline (GSK, Stevenage, UK) and used in their optimal concentration: GNF2 10 µM, Nilotinib 10 µM, Nintedanib 1 µM, Erlotinib 10 µM and Dasatinib 0.1 µM, as determined by performing concentration series studies in an ECIS analysis (data not shown). PF-6260933 (Selleckem) was dissolved in sterile water in a concentration of 3 µM.

Antibodies against the following proteins were used: MAP4K4 (HGK, #3485 1:1000), VE-cadherin XP (D87F2,#2500 1:200-1000), phospho-Ezrin(Thr567)/Radixin(Thr564)/Moesin(Thr558) (#3141S 1:500–1:1000), Ezrin/Radixin/Moesin (#3142 1:500–1:1000), pMLC (#3671 1:2000), P44/42 MAP Kinase (ERK1/2) (#9102 1:2000) vinculin (#4650 1:5000) (all Cell Signaling), VE-cadherin (SC-6458, Santa Cruz Biotechnology, 1:500–1:1000), integrin β1 (12G10, ab30394, Abcam 1:200–1:500), ABL2 (M09, clone 5C6, Abnova 1:500–1:1000). The following small interference RNAs (siRNAs) were purchased: ON-TARGET plus non-targeting pool (siNT); 5′-GAGCCAAAUUUCCUAA-3′ siARG #2; 5′-GACCAACUCUGGCU-UGUUA-3′ ON-TARGET plus human MAP4K4 (siMAP4K4 #10, 11, 12, 13 or pool); ON-TARGET plus human MINK1 pool (siMAP4K6); ON-Target plus human TNIK pool (siMAP4K7) (all GE-Healthcare/Dharmacon); human moesin siRNA (sc-35955) and human ezrin siRNA (sc-35349) both Santa Cruz Biotechnology Inc.

Endothelial cell culture

Human umbilical vein endothelial cells (HUVECs) were purchased from Lonza or freshly isolated from umbilical cords of healthy donors. Cells were isolated and characterized as previously described (Jaffe et al., 1973). Human pulmonary microvascular endothelial cells (PMVECs) were isolated and cultured from healthy donors, approved by the institutional review board of the VU University Medical Center following principles outlined in the Declaration of Helsinki and consent was given. Isolation and culturing of human pulmonary microvascular endothelial cells (PMVECs) from healthy donor lungs was described by our group previously (Szulcek et al., 2016). HUVECs were cultured in M199 medium supplemented with 100 U/ml penicillin and 100 µg/ml streptomycin, and 2 mM L-glutamine (all Biowhittaker/Lonza, Verviers, Belgium), 10% heat-inactivated human serum (Sanquin blood supply, Amsterdam, The Netherlands), 10% heat-inactivated new-born calf serum (NBCS, Gibco, Grand Island, NY), 150 µg/ml crude endothelial cell growth factor (prepared from bovine brains) and 5 U/ml heparin (Leo pharmaceutical products, Weesp, The Netherlands), cultured at 37°C and 5% CO_2, with a medium change every other day. Cells were used for experiments in passage 1 or 2.

Transfection with small interfering RNAs

Subconfluent HUVECs (80% confluency) were transfected with 10% NBCS in M199 containing 25 nM Dharmafect 1 (Dharmacon/GE-healthcare) and 25 nM of siRNA. After 16 h of transfection, medium was changed to regular culture medium to avoid toxicity. Experiments were performed 72 h after transfection. Efficiency of transfection was evaluated by western blot analysis or PCR of whole-cell lysates.

Endothelial barrier function assays

Endothelial barrier function was measured by performing an electrical cell-substrate impedance sensing (ECIS) or macromolecule passage assay. HUVECs were seeded to immediate confluency on gelatin-coated ECIS arrays (Applied Biophysics, Troy, NY). Culture medium was renewed 24 h after seeding, while experiments were performed 48 h after seeding. Before thrombin stimulation, cells were incubated with M199 medium (Biowhittaker/Lonza, Verviers, Belgium) containing 1% human serum albumin (HSA, Sanquin CLP) and the compounds in designated concentrations. After 60–90 min of pre-incubation, thrombin was added to the wells in a final concentration of 1 U/ml (Sigma-Aldrich). HUVECs

were transfected 24 h after seeding using Dharmafect 1 and siRNAs for 16 h, followed by medium change.

For analyzing cell adhesion, cells were serum starved and pre-incubated with DMSO or bosutinib (1 µM) for 1 h in m199 containing 1% HSA after which cells were detached by trypsin and counted. A final number of 10,000 cells per well was seeded on gelatin-coated ECIS arrays and resistance was measured during the adhesion and growth phase for 2 h.

After pre-incubation with DMSO (0.01%) or bosutinib (1 µM) in 1% HSA for 90 min, integrin-blocking peptides GRGDNP (AS-62049 AnaSpec) and GRGDSP (AS-22945 AnaSpec) dissolved in 1% HSA were added in increasing concentrations of 0–4 mM on primary HUVEC monolayers in ECIS. After 60 min, a plateau phase was reached and 1 U/ml thrombin was added. When the concentration of the peptides exceeded 500 µM, the barrier could not recover over time and we therefore used an optimal concentration of 450 µM in subsequent experiments.

Macromolecular passage

HUVECs were seeded to confluency on top of 0.33 cm^2 gelatin-coated ThinCerts® cell culture inserts (Greiner Bio-one) with a pore-size of 3.0 µm and cultured in EGM-2 medium with a medium change every other day. When a solid barrier was formed, defined as the absence of medium leak, cells were pre-incubated for 1 h with EBM medium containing 1% HSA and the compounds in designated concentrations. For stimulation, medium in the upper compartment was replaced by 1% HAS in EBM containing 5 µg/ml horseradish peroxidase (HRP) and 1 U/ml thrombin or a vehicle control. Also 1% HAS in EBM was added to the lower compartment. Samples were taken from the lower compartment for HRP quantification at several time points.

Cells were transfected 24 h before transfer to 1% gelatin-coated ThinCerts®. HRP was quantified by measuring absorption after adding tetramethylbenzidine (Upstate/Millipore) and sulfuric acid to stop the reaction.

Kinase binding assay

In vitro kinase binding assay was performed by GSK following standard procedures. In short, base reaction buffer was prepared, containing 20 mM HEPES pH 7.5, 10 mM $MgCl_2$, 1 mM EGTA, 0.02% Brij35, 0.02 mg/ml BSA, 0.1 mM Na_3VO_4, 2 mM DTT and 1% DMSO. The indicated kinase was mixed with substrate solution and compounds were delivered into the kinase reaction mixture by Acoustic technology (Echo550; nanoliter range). To initiate the kinase binding reaction, [^{33}P]ATP was added, incubated for 2 h at room temperature and reactions were spotted onto P81 ion exchange paper. Kinase activity against 396 kinases was detected by filter-binding method. Thresholds for kinase inhibition of ≥75% at 10 nM bosutinib and ≤50% at 10 µM imatinib were chosen to select candidate kinases.

Protein analysis

For protein analysis, cells were seeded in 5 or 10 cm^2 culture wells and possibly transfected as described above. When cells reach confluency they were washed with ice-cold PBS and whole-cell lysates were collected by scraping the cells in 2× concentrated SDS sample buffer. Protein samples were separated on 8 or 12.5% SDS page gels or 4–12% precast gels (Bio-Rad) by electrophoresis and transferred onto nitrocellulose membranes. Protein analysis was performed by incubation of the nitrocellulose membranes with the designated antibodies. Bands were visualized with enhanced chemiluminescence (Amersham/GE Healthcare) on a AI600 machine (Amersham/GE Healthcare) and intensity was quantified using ImageQuant TL software (GE Healthcare).

Immunofluorescence imaging of cultured endothelial cells

Cells were seeded on 2 cm^2 and 12 mm glass coverslips (Menzel), coated with 1% gelatin and crosslinked with 0.5% glutaraldehyde (Sigma-Aldrich). Transfected cells were seeded ∼24 h after the start of transfection. Untransfected cells were seeded and grown to confluence in 48 h with a medium change the day after seeding. Cells were pre-incubated with 1% HAS in M199 for 1 h with bosutinib (1 µM) or DMSO, thrombin was added to the wells in a final concentration of 1 U/ml. After 2–15 min, cells were fixated with warm (37°C) 4% paraformaldehyde (Sigma-Aldrich) and put on ice for 15 min. Cells were permeabilized with 0.2% Triton X-100 in PBS (Sigma-Aldrich) and blocked for 30 min with 0.1% HSA. Subsequently, coverslips were stained with primary antibodies (in 0.1% HAS in PBS) for 1–2 h at room temperature. After washing three times, the cells were incubated with FITC or Cy5-labeled secondary antibodies (anti-rabbit-IgG or anti-mouse-IgG at 1:100 in 0.1% HAS in PBS) and F-actin was visualized using labeled phalloidin [in 0.1% HAS in PBS (Tebu bio)] at room temperature for 1–2 h. After washing, the cells were incubated with DAPI (Thermo Fisher Scientific) at room temperature for 30 min. Coverslips were mounted with Mowiol4-88/DABCO solution (Calbiochem, Sigma Aldrich). Confocal scanning microscopy was performed on a Nikon A2R confocal microscope (Nikon). Images were analyzed and processed using ImageJ. Gap area was quantified using the freehand selection tool in the VE-cadherin staining images. The density and number of FAs in total and at the periphery relative to the cell were quantified using ImageJ. In short, images were converted into 8-bit grayscale, foreground/background colors were inverted, and the threshold was adjusted. The analyze particles function was used to select and measure focal adhesions. FAs were considered peripheral when present at >2/3 of the distance from nucleus to cell membrane. The number of FAs was counted and corrected for the number of nuclei. VE-cadherin intensity was quantified using the line-measurement from the cytosol to cell membrane in ImageJ. Individual peak intensity was divided by individual cytosolic intensity from four positions per picture and five pictures per condition, and averaged in four separate experiments.

Live fluorescence microscopy of FA dynamics

HUVECs were transduced with third-generation lentivirus derived from pRRL-Vinculin-GFP plasmid as previously described (Huveneers et al., 2012). Cells were plated in a density of 50,000 cells/ml on Lab-Tek chambered 1.0 borosilicated coverglass slides coated with 3 mg/ml fibronectin. The next day, cells were imaged using total internal reflection fluorescence (TIRF) microscopy. Immunofluorescence VE-cadherin antibody (BD Biosciences; 647 anti-human CD144 cat. no. 561567) was added 30 min before imaging in Movie 3 to illustrate cell responses in a monolayer. After 60–90 min of DMSO or bosutinib treatment, thrombin was added and imaging continued for 30 min with intervals of 30 s. Cells were imaged using a NIKON Eclipse TI equipped with a 60× Apo TIRF oil objective (NA 1.49) and an Andor Zyla 4.2 plus sCMOS camera. An Okolab cage incubator and humidified CO_2 gas chamber set to 37°C and 5% CO_2 were used during the imaging process. Original data from single cells without VE-cadherin staining in Movies 1 and 2 was uploaded on the FA analysis server (http://faas.bme.unc.edu/) (Berginski et al., 2011; Berginski and Gomez, 2013) for quantification of FA dynamics. Images were enhanced for display with an unsharp mask filter and by adjusting brightness and contrast settings. In brief, FAs were identified based on GFP–vinculin positivity within thresholded images. Dynamic properties [(dis)assembly rate and longevity] of FAs was obtained by the tracking of changes in intensity of the fluorescence from single adhesions through subsequent image frames; 9–16 images per condition were imaged and analyzed out of two experiments. Please note that in Movie 3, the VE-cadherin intensity was equalized and enhanced against bleaching.

MTT cell viability assay

MTT [3-(4,5-dimethylthiazol-2-yl)-2,5-diphenyl-2H-tetrazolium bromide] was purchased from Abcam, ab211091 lot number GR3285654-2. HUVECs were grown as previously described on 1% gelatin-coated 96-well flat bottom plates in a density of 50,000 cells/well. After 48 h, cells were incubated with 0, 0.1 µM, 1 µM and 10 µM bosutinib in serum starved medium, or 500 µM H_2O_2 as positive control for 120 min. MTT reagent and MTT solvent were added following the manufacturer's protocol. Absorbance was read at 590 nm. Percentage cell viability was calculated as [(sample background)/control]×100.

PCR

RNA was isolated and cDNA was generated using an RNA isolation kit (Zymo Research Direct-zol MiniPrep R2050) and iScript cDNA synthesis kit (Bio-Rad, #170-8891) according to manufacturer's instructions. For PCR reactions FAST SYBR Green Master Mix (Thermo Fisher Scientific,

4385612) was used. qPCR was then performed to quantify the expression of MAP4K4, MAP4K5, MAP4K6 and MAP4K7. GAPDH and TBP were used as housekeeping genes to normalize for the amount of total RNA per sample. Gene expression was determined by the LightCycler 480 Instrument II (Roche Applied Science, Penzberg, Germany), and the reactions were prepared using Light Cycler SYBR Green IMaster (Roche Applied Science). Primers were: MAP4K4, F1, 5′-AAGATGTACGGCC-ACCTCAC-3′ and R1, 5′-ATTCCGTTTCACCATTGCTC-3′; MAP4K5, F1, 5′-GCAGCCAGCAGTTAGATTCC-3′ and R1, 5′-TCCAGAAAGC-CAACACACTG-3′; MAP4K6, F1, 5′-GAGAACAGCAAAGGCCAAAG-3′ and R1, 5′-TGACCACAGAACCCTTCCTC-3′; MAP4K7, F1, 5′-TC-ACCTGCACCAGCATAAAG-3′ and R1, 5′-TGCCATCCAGTAGGGA-GTTC-3′; TBP, c472-01F, 5′-AGTTCTGGGATTGTACCGCA-3′ and c610-01R, 5′-TCCTCATGATTACCGCAGCA-3′.

Animals

The Ethical Committee for Animal Experiments of the Academic Medical Center (Amsterdam, The Netherlands) approved all animal protocols (LEICA-132AE) conform to the guidelines from Directive 2010/63/EU of the European Parliament on the protection of animals used for scientific purposes. Experiments were performed in 42 male C57/Bl6 mice with a mean±s.d. body weight of 23.5±1.7 g purchased from Charles River Laboratories (The Netherlands). Animals were handled 1 week before the experiment to diminish stress activation. Housing took place in a specific-pathogen free facility on a 12-h-light–12-h-dark cycle and animals were allowed to take food and tap water *ad libitum*. Animals were randomized into a control group (NaCl, n=6), LPS group (n=9) and LPS+bosutinib group (n=9). For the additional experiment assessing Evan's Blue extravasation, each group consisted of n=6.

Direct lung injury model

At baseline, mice were weighed and labeled, followed by intranasal administration of lipopolysaccharide (LPS; 5 mg/kg of body weight, *E. coli*, serotype: 0127:B8, Sigma-Aldrich) diluted in 50 µl NaCl 0.9% (NaCl, Braun, Germany) or 50 µl NaCl 0.9% (NaCl group) under isoflurane anesthesia (2–4%). Concomitantly, mice received either bosutinib (Selleck chemicals s104, 20 mg/kg of body weight dissolved in a solution buffer (2% DMSO, 30% PEG, 5% Tween in MQ) or solution buffer only (control and LPS group) in a total volume of 500 µl intraperitoneally (i.p.). After 6 h, all animals were sacrificed under general anesthesia [KDA mix; 1.26 ml 100 mg/ml ketamine (Anesketin, EuroVetAnimal Health B.V., Bladel, The Netherlands), 0.2 ml 0.5 mg/ml dexmedetomidine (Pfizer Animal Health, B.V., Capelle a/d Ijssel, The Netherlands) and 1 ml 0.5 mg/ml atropine (Pharmachemie, Haarlem, The Netherlands)] in 5 ml 0.9% NaCl by exsanguination via the vena cava inferior. Whole blood was collected a heparin-coated syringe and centrifuged for 10 min at 4000 rpm at 4°C (Eppendorf, microcentrifuge). Plasma was obtained and stored at −80°C for further analyses. Bronchoalveolar lavage fluid (BALF) was obtained from the left lung. The superior and inferior lobe of the right lung were excised for histopathologic examination. The two middle lobes were used for the lung weight/body weight ratio.

Assessment of lung injury

After ligating the hilum of the right lung, the trachea was cannulated and the left lung was washed three times with 0.3 ml saline to obtain BALF. BALF was centrifuged for 10 min at 300 ***g*** at 4°C (Eppendorf, microcentrifuge) and stored at −80°C for further analyses. The superior and inferior lobe of the right lung were excised, instilled with 4% paraformaldehyde and embedded in paraffin for histopathological assessment. The two middle lobes were removed and weighed together directly after resection followed by incubation in a 37°C stove for determination of the dry weight after 7 days. Total protein content in BALF was determined using the Lowry method. Total cell counts in BALF were evaluated with the Beckman Coulter (Fullerton, CA, USA). Differential cell counts were performed on cytospin preparations (Shandon CytospinR 4 Cytocentrifuge; Thermo Electron Corporation) and stained with a modified Giemsa stain (DiffQuick, Dade Behring AG, Duedingen, Switzerland). The inflammatory cytokine Interleukin (IL)-6 was assessed in plasma and BALF and tumor necrosis factor (TNF)-α was measured in BALF using a mouse-specific ELISA kit (R&D systems; Minneapolis, MN, USA) according to manufacturer's instructions. Histologic evidence of lung injury was assessed from hematoxylin and eosin-stained lung sections by using an established histopathologic score from 0 (no injury) to 3 (severe injury). This score consists of endothelialitis, bronchitis, edema formation, interstitial inflammation and hemorrhage which was scored by a pathologist who was blind to the experimental conditions.

Evans Blue extravasation

Lung permeability was determined by assessing tissue accrual of Evans Blue (Sigma Chemical Co.) as previously described (Green et al., 1988). Lung injury was induced and treatment administered as described above. After 5 h, mice were anesthetized with isoflurane and 200 µl of 0.5% Evans Blue was administered via the penile vein. After 1 h, animals were anesthetized as described above and killed through blood collection from the heart. 5 ml of 0.9% NaCl was injected in the inferior vena cava to rinse the circulation. The right lung was collected, snapfrozen in liquid nitrogen and stored at −80°C. The left lung, kidneys and heart were placed in 300 µl formamide at 55°C to extract the Evan's Blue from the tissue. After 48 h, the organs were placed in an incubator at 90°C for 24 h to calculate and correct for dry weight. Evans Blue concentration in supernatants was quantified by a dual wavelength spectrophotometric method at 620 nm and 740 nm absorbance, and corrected for the dry weight.

Neutrophil isolation

Polymorphonuclear neutrophils (PMNs) were isolated from whole blood derived from healthy donors. All volunteers signed an informed consent, under the rules and legislation in place within the Netherlands and maintained by the Sanquin Medical Ethical Committee. The rules and legislations are based on the Declaration of Helsinki and guidelines for Good Clinical Practice. Whole blood was diluted (1:1) with 5% (v/v) tri-natrium citrate in PBS. Diluted whole blood was pipetted carefully onto 12.5 ml Percoll (room temperature) 1.076 g/ml. Tubes were centrifuged (Rotanta 96R) at 800 ***g***, slow start, low brake for 20 min. Bottom fraction containing PMNs was further processed by erythrocyte lysis in ice-cold isotonic lysis buffer (155 mM NH_4Cl, 10 mM $KHCO_3$, 0.1 mM EDTA, pH 7.4 in Milli-Q (Millipore). PMNs were centrifuged at 500 ***g*** for 5 min at 4°C and incubated, again with lysis buffer, for 5 min on ice. After another centrifugation at 500 ***g*** for 5 min at 4°C, PMNs were washed once with PBS and centrifuged again at 500 ***g*** for 5 min at 4°C before resuspension in HEPES medium [20 mM HEPES pH 7.4, 132 mM NaCl, 6 mM KCl, 1 mM $CaCl_2$, 1 mM $MgSO_4$, 1.2 mM K_2HPO_4 and 5 mM glucose (all from Sigma-Aldrich) and 0.4% (w/v) human serum albumin (Sanquin Reagents)]. PMNs count and purity was determined by cell counter (Casy) and cells kept at room temperature for no longer than 4 h before use.

Trans-endothelial migration of neutrophils

Primary lung microvascular endothelial cells (PMVECs) were cultured on fibronectin-coated ibidi slides at a density of 0.5×10^5 per channel (µ-slide VI0.4, Ibidi). After 72 h, cells were stimulated for 4 h with 100 ng/ml of LPS (Sigma-Aldrich) and 1 µM DMSO or bosutinib. Freshly isolated PMNs were suspended in HEPES medium and activated by 30 min incubation at 37°C. Flow channels were connected to a perfusion system and exposed to 0.5 ml/min HEPES medium pH 7.4, with shear flow (0.8 dyn/cm^2), and 10^6 cells/channel of heat-activated PMNs were injected. Leukocyte–endothelial interactions were recorded for 20 min at 0.2 frames/s by a Zeiss Observer Z1 microscope. All live imaging was performed at 37°C in the presence of 5% CO_2. Transmigrated PMNs were distinguished from those adhering to the apical surface of the endothelium by their transition from bright- to phase-dark morphology. The number of transmigrated PMNs was manually quantified using ImageJ.

Statistical analysis

Data are represented as mean±s.d. Comparison of two conditions were tested by Student's t-test. Comparison of more than two conditions were tested by one-way ANOVA or repeated measures ANOVA. A Dunnett's

post hoc test was used when conditions were compared to one control, and a Bonferroni post hoc test was used when multiple conditions were compared to multiple conditions, unless indicated otherwise. *P*-values were considered statistically significant if $P<0.05$. Analysis was performed using Graphpad prism software.

Acknowledgements
We thank F. Breijer, M. A. W. Maas and N. Bogunovic for helping with experiments.

Competing interests
The authors declare no competing or financial interests.

Author contributions
Conceptualization: L.B., M.C.A.P., J.J., J.L., J.D.v.B., R.H.B., P.R.T., H.J.B., V.W.M.v.H., P.L.H., J.A.; Methodology: L.B., M.C.A.P., J.J., J.L., R.H.B., S.H., J.A.; Software: L.B., J.L., S.H.; Validation: L.B., R.H.B., H.J.B., V.W.M.v.H., P.L.H., J.A.; Formal analysis: L.B., M.C.A.P., J.J., J.L., R.H.B., S.H.; Investigation: L.B., M.C.A.P., J.J., S.K.H.M., J.D.v.B., P.R.T., J.S.M.v.B., S.H., J.A.; Resources: J.J., S.K.H.M., J.D.v.B., P.R.T., S.H., H.J.B., P.L.H., J.A.; Data curation: L.B., M.C.A.P., J.J., J.L., S.K.H.M., J.D.v.B., J.S.M.v.B.; Writing - original draft: L.B., M.C.A.P., J.J.; Writing - review & editing: L.B., J.L., R.H.B., P.R.T., S.H., H.J.B., V.W.M.v.H., P.L.H., J.A.; Visualization: L.B., M.C.A.P., J.J., S.H., J.A.; Supervision: S.H., H.J.B., V.W.M.v.H., P.L.H., J.A.; Project administration: H.J.B., P.L.H., J.A.; Funding acquisition: P.R.T., S.H., H.J.B., P.L.H., J.A.

Funding
This work was supported by the Netherlands Cardiovascular Research Initiative: the Dutch Heart Foundation, Dutch Federation of University Medical Centers, the Netherlands Organization for Health Research and Development, and the Royal Netherlands Academy of Sciences Grant 2012-08 awarded to the Phaedra consortium. J.A. was funded by Dutch Heart Foundation grant number 2014T064. S.H. was supported by a Nederlandse Organisatie voor Wetenschappelijk Onderzoek (NOW) VIDI grant ZonMW; 016.156.327.

Supplementary information
Supplementary information available online at
http://jcs.biologists.org/lookup/doi/10.1242/jcs.240077.supplemental

Peer review history
The peer review history is available online at
https://jcs.biologists.org/lookup/doi/10.1242/jcs.240077.reviewer-comments.pdf

References

Adyshev, D. M., Dudek, S. M., Moldobaeva, N., Kim, K.-M., Ma, S.-F., Kasa, A., Garcia, J. G. N. and Verin, A. D. (2013). Ezrin/radixin/moesin proteins differentially regulate endothelial hyperpermeability after thrombin. *Am. J. Physiol. Lung Cell. Mol. Physiol.* **305**, L240-L255. doi:10.1152/ajplung.00355.2012

Aman, J., van Bezu, J., Damanafshan, A., Huveneers, S., Eringa, E. C., Vogel, S. M., Groeneveld, A. B. J., Vonk Noordegraaf, A., van Hinsbergh, V. W. M. and van Nieuw Amerongen, G. P. (2012). Effective treatment of edema and endothelial barrier dysfunction with imatinib. *Circulation* **126**, 2728-2738. doi:10.1161/CIRCULATIONAHA.112.134304

Aman, J., Peters, M. J. L., Weenink, C., van Nieuw Amerongen, G. P. and Vonk Noordegraaf, A. (2013). Reversal of vascular leak with imatinib. *Am. J. Respir. Crit. Care. Med.* **188**, 1171-1173. doi:10.1164/rccm.201301-0136LE

Ammirati, M., Bagley, S. W., Bhattacharya, S. K., Buckbinder, L., Carlo, A. A., Conrad, R., Cortes, C., Dow, R. L., Dowling, M. S., El-Kattan, A. et al. (2015). Discovery of an in vivo tool to establish proof-of-concept for MAP4K4-based antidiabetic treatment. *ACS Med. Chem. Lett.* **6**, 1128-1133. doi:10.1021/acsmedchemlett.5b00215

Amsellem, V., Dryden, N. H., Martinelli, R., Gavins, F., Almagro, L. O., Birdsey, G. M., Haskard, D. O., Mason, J. C., Turowski, P. and Randi, A. M. (2014). ICAM-2 regulates vascular permeability and N-cadherin localization through ezrin-radixin-moesin (ERM) proteins and Rac-1 signalling. *Cell Commun. Signal.* **12**, 12. doi:10.1186/1478-811X-12-12

Baumgartner, M., Sillman, A. L., Blackwood, E. M., Srivastava, J., Madson, N., Schilling, J. W., Wright, J. H. and Barber, D. L. (2006). The Nck-interacting kinase phosphorylates ERM proteins for formation of lamellipodium by growth factors. *Proc. Natl. Acad. Sci. USA* **103**, 13391-13396. doi:10.1073/pnas.0605950103

Berginski, M. E. and Gomez, S. M. (2013). The Focal Adhesion Analysis Server: a web tool for analyzing focal adhesion dynamics. *F1000 Res* **2**, 68. doi:10.12688/f1000research.2-68.v1

Berginski, M. E., Vitriol, E. A., Hahn, K. M. and Gomez, S. M. (2011). High-resolution quantification of focal adhesion spatiotemporal dynamics in living cells. *PLoS ONE* **6**, e22025. doi:10.1371/journal.pone.0022025

Carneiro, P. J., Clevelario, A. L., Padilha, G. A., Silva, J. D., Kitoko, J. Z., Olsen, P. C., Capelozzi, V. L., Rocco, P. R. M. and Cruz, F. F. (2017). Bosutinib therapy ameliorates lung inflammation and fibrosis in experimental silicosis. *Front. Physiol.* **8**, 159. doi:10.3389/fphys.2017.00159

Chuang, H.-C., Wang, X. and Tan, T.-H. (2016). MAP4K family kinases in immunity and inflammation. *Adv. Immunol.* **129**, 277-314. doi:10.1016/bs.ai.2015.09.006

Cortes, J. E., Gambacorti-Passerini, C., Deininger, M. W., Mauro, M. J., Chuah, C., Kim, D.-W., Dyagil, I., Glushko, N., Milojkovic, D., le Coutre, P. et al. (2018). Bosutinib versus imatinib for newly diagnosed chronic myeloid leukemia: results from the randomized BFORE trial. *J. Clin. Oncol.* **36**, 231-237. doi:10.1200/JCO.2017.74.7162

Dejana, E. and Giampietro, C. (2012). Vascular endothelial-cadherin and vascular stability. *Curr. Opin Hematol.* **19**, 218-223. doi:10.1097/MOH.0b013e3283523e1c

Fehon, R. G., Mcclatchey, A. I. and Bretscher, A. (2010). Organizing the cell cortex: the role of ERM proteins. *Nat. Rev. Mol. Cell Biol.* **11**, 276-287. doi:10.1038/nrm2866

Filewod, N. C. and Lee, W. L. (2019). Inflammation without vascular leakage science fiction no longer? *Am. J. Respir. Crit. Care. Med.* **200**, 1472-1476. doi:10.1164/rccm.201905-1011CP

Gavard, J. (2013). Endothelial permeability and VE-cadherin: a wacky comradeship. *Cell Adh. Migr.* **7**, 465-471. doi:10.4161/cam.27330

Giancotti, F. G. (2000). Complexity and specificity of integrin signalling. *Nat. Cell Biol.* **2**, E13-E14. doi:10.1038/71397

Gorbunova, E. E., Gavrilovskaya, I. N., Pepini, T. and Mackow, E. R. (2011). VEGFR2 and Src kinase inhibitors suppress Andes virus-induced endothelial cell permeability. *J. Virol.* **85**, 2296-2303. doi:10.1128/JVI.02319-10

Gover-Proaktor, A., Granot, G., Pasmanik-Chor, M., Pasvolsky, O., Shapira, S., Raz, O., Raanani, P. and Leader, A. (2018). Bosutinib, dasatinib, imatinib, nilotinib, and ponatinib differentially affect the vascular molecular pathways and functionality of human endothelial cells. *Leuk. Lymphoma* **60**, 189-199. doi:10.1080/10428194.2018.1466294

Green, T. P., Johnson, D. E., Marchessault, R. P. and Gatto, C. W. (1988). Transvascular flux and tissue accrual of Evans blue: effects of endotoxin and histamine. *J. Lab. Clin. Med.* **111**, 173-183.

Hakanpaa, L., Kiss, E. A., Jacquemet, G., Miinalainen, I., Lerche, M., Guzman, C., Mervaala, E., Eklund, L., Ivaska, J. and Saharinen, P. (2018). Targeting beta1-integrin inhibits vascular leakage in endotoxemia. *Proc. Natl. Acad. Sci. USA.* **115**, E6467-E6476. doi:10.1073/pnas.1722317115

Heyen, J. R., Hu, W., Jamieson, J., Thibault, S., Batugo, M., Loi, C.-M., Burns-Naas, L. A., Mcharg, A. D. and Jessen, B. (2013). Cardiovascular differentiation of imatinib and bosutinib in the rat. *Int. J. Hematol.* **98**, 597-607. doi:10.1007/s12185-013-1453-2

Huang, C., Jacobson, K. and Schaller, M. D. (2004). MAP kinases and cell migration. *J. Cell Sci.* **117**, 4619-4628. doi:10.1242/jcs.01481

Huang, H., Tang, Q., Chu, H., Jiang, J., Zhang, H., Hao, W. and Wei, X. (2014). MAP4K4 deletion inhibits proliferation and activation of CD4(+) T cell and promotes T regulatory cell generation in vitro. *Cell. Immunol.* **289**, 15-20. doi:10.1016/j.cellimm.2014.02.006

Huveneers, S., Oldenburg, J., Spanjaard, E., van der Krogt, G., Grigoriev, I., Akhmanova, A., Rehmann, H. and DE Rooij, J. (2012). Vinculin associates with endothelial VE-cadherin junctions to control force-dependent remodeling. *J. Cell Biol.* **196**, 641-652. doi:10.1083/jcb.201108120

Hynes, R. O. (2002). Integrins: bidirectional, allosteric signaling machines. *Cell* **110**, 673-687. doi:10.1016/S0092-8674(02)00971-6

Jaffe, E. A., Nachman, R. L., Becker, C. G. and Minick, C. R. (1973). Culture of Human Endothelial cells derived from Umbilical veins. Identification by morphologic and immunologic criteria. *J. Clin. Invest.* **52**, 2745-2756. doi:10.1172/JCI107470

Kapp, T. G., Rechenmacher, F., Neubauer, S., Maltsev, O. V., Cavalcanti-Adam, E. A., Zarka, R., Reuning, U., Notni, J., Wester, H.-J., Mas-Moruno, C. et al. (2017). A comprehensive evaluation of the activity and selectivity profile of ligands for RGD-binding integrins. *Sci. Rep.* **7**, 39805. doi:10.1038/srep39805

Khoury, H. J., Cortes, J. E., Kantarjian, H. M., Gambacorti-Passerini, C., Baccarani, M., Kim, D.-W., Zaritskey, A., Countouriotis, A., Besson, N., Leip, E. et al. (2012). Bosutinib is active in chronic phase chronic myeloid leukemia after imatinib and dasatinib and/or nilotinib therapy failure. *Blood* **119**, 3403-3412. doi:10.1182/blood-2011-11-390120

Komarova, Y. A., Kruse, K., Mehta, D. and Malik, A. B. (2017). Protein interactions at endothelial junctions and signaling mechanisms regulating endothelial permeability. *Circ. Res.* **120**, 179-206. doi:10.1161/CIRCRESAHA.116.306534

Kong, J. H., Khoury, H. J., Kim, A. S., Hill, B. G. and Kota, V. (2017). The safety of Bosutinib for the treatment of chronic myeloid leukemia. *Expert Opin. Drug Saf.* **16**, 1203-1209. doi:10.1080/14740338.2017.1363176

Lee, W. L. and Slutsky, A. S. (2010). Sepsis and endothelial permeability. *N. Engl. J. Med.* **363**, 689-691. doi:10.1056/NEJMcibr1007320

Machida, N., Umikawa, M., Takei, K., Sakima, N., Myagmar, B.-E., Taira, K., Uezato, H., Ogawa, Y. and Kariya, K.-I. (2004). Mitogen-activated protein kinase

kinase kinase kinase 4 as a putative effector of Rap2 to activate the c-Jun N-terminal kinase. *J. Biol. Chem.* **279**, 15711-15714. doi:10.1074/jbc.C300542200

Matthay, M. A., Zemans, R. L., Zimmerman, G. A., Arabi, Y. M., Beitler, J. R., Mercat, A., Herridge, M., Randolph, A. G. and Calfee, C. S. (2019). Acute respiratory distress syndrome. *Nat. Rev. Dis. Primers* **5**, 18. doi:10.1038/s41572-019-0069-0

Mehta, D. and Malik, A. B. (2006). Signaling mechanisms regulating endothelial permeability. *Physiol. Rev.* **86**, 279-367. doi:10.1152/physrev.00012.2005

Pannekoek, W.-J., Linnemann, J. R., Brouwer, P. M., Bos, J. L. and Rehmann, H. (2013). Rap1 and Rap2 antagonistically control endothelial barrier resistance. *PLoS ONE* **8**, e57903. doi:10.1371/journal.pone.0057903

Pulous, F. E. and Petrich, B. G. (2019). Integrin-dependent regulation of the endothelial barrier. *Tissue Barriers* **7**, 1685844. doi:10.1080/21688370.2019.1685844

Pulous, F. E., Grimsley-Myers, C. M., Kansal, S., Kowalczyk, A. P. and Petrich, B. G. (2019). Talin-dependent integrin activation regulates VE-cadherin localization and endothelial cell barrier function. *Circ. Res.* **124**, 891-903. doi:10.1161/CIRCRESAHA.118.314560

Rizzo, A. N., Aman, J., van Nieuw Amerongen, G. P. and Dudek, S. M. (2015). Targeting Abl kinases to regulate vascular leak during sepsis and acute respiratory distress syndrome. *Arterioscler. Thromb. Vasc. Biol.* **35**, 1071-1079. doi:10.1161/ATVBAHA.115.305085

Roth Flach, R. J., Skoura, A., Matevossian, A., Danai, L. V., Zheng, W., Cortes, C., Bhattacharya, S. K., Aouadi, M., Hagan, N., Yawe, J. C. et al. (2015). Endothelial protein kinase MAP4K4 promotes vascular inflammation and atherosclerosis. *Nat. Commun.* **6**, 8995. doi:10.1038/ncomms9995

Shattil, S. J., Kim, C. and Ginsberg, M. H. (2010). The final steps of integrin activation: the end game. *Nat. Rev. Mol. Cell Biol.* **11**, 288-300. doi:10.1038/nrm2871

Song, J., Zhang, X., Buscher, K., Wang, Y., Wang, H., Di Russo, J., Li, L., Lütke-Enking, S., Zarbock, A., Stadtmann, A. et al. (2017). Endothelial basement membrane Laminin 511 contributes to endothelial junctional tightness and thereby inhibits leukocyte transmigration. *Cell Rep.* **18**, 1256-1269. doi:10.1016/j.celrep.2016.12.092

Su, G., Hodnett, M., Wu, N., Atakilit, A., Kosinski, C., Godzich, M., Huang, X. Z., Kim, J. K., Frank, J. A., Matthay, M. A. et al. (2007). Integrin αvβ5 regulates lung vascular permeability and pulmonary endothelial barrier function. *Am. J. Respir. Cell Mol. Biol.* **36**, 377-386. doi:10.1165/rcmb.2006-0238OC

Su, G., Atakilit, A., Li, J. T., Wu, N., Bhattacharya, M., Zhu, J., Shieh, J. E., Li, E., Chen, R., Sun, S. et al. (2012). Absence of integrin αvβ3 enhances vascular leak in mice by inhibiting endothelial cortical actin formation. *Am. J. Respir. Crit. Care. Med.* **185**, 58-66. doi:10.1164/rccm.201108-1381OC

Szulcek, R., Happé, C. M., Rol, N., Fontijn, R. D., Dickhoff, C., Hartemink, K. J., Grünberg, K., Tu, L., Timens, W., Nossent, G. D. et al. (2016). Delayed microvascular shear adaptation in pulmonary arterial hypertension. Role of platelet endothelial cell adhesion molecule-1 cleavage. *Am. J. Respir. Crit. Care. Med.* **193**, 1410-1420. doi:10.1164/rccm.201506-1231OC

Tachibana, K., Haghparast, S. M. A. and Miyake, J. (2015). Inhibition of cell adhesion by phosphorylated Ezrin/Radixin/Moesin. *Cell Adh. Migr.* **9**, 502-512. doi:10.1080/19336918.2015.1113366

Tripolitsioti, D., Kumar, K. S., Neve, A., Migliavacca, J., Capdeville, C., Rushing, E. J., Ma, M., Kijima, N., Sharma, A., Pruschy, M. et al. (2018). MAP4K4 controlled integrin β1 activation and c-Met endocytosis are associated with invasive behavior of medulloblastoma cells. *Oncotarget* **9**, 23220-23236. doi:10.18632/oncotarget.25294

Tuinman, P. R., Müller, M. C., Jongsma, G., Hegeman, M. A. and Juffermans, N. P. (2013). High-dose acetylsalicylic acid is superior to low-dose as well as to clopidogrel in preventing lipopolysaccharide-induced lung injury in mice. *Shock* **40**, 334-338. doi:10.1097/SHK.0b013e3182a384f0

Vitorino, P., Yeung, S., Crow, A., Bakke, J., Smyczek, T., West, K., Mcnamara, E., Eastham-Anderson, J., Gould, S., Harris, S. F. et al. (2015). MAP4K4 regulates integrin-FERM binding to control endothelial cell motility. *Nature* **519**, 425-430. doi:10.1038/nature14323

Wang, Y., Jin, G., Miao, H., Li, J. Y.-S., Usami, S. and Chien, S. (2006). Integrins regulate VE-cadherin and catenins: dependence of this regulation on Src, but not on Ras. *Proc. Natl. Acad. Sci. USA* **103**, 1774-1779. doi:10.1073/pnas.0510774103

Wessel, F., Winderlich, M., Holm, M., Frye, M., Rivera-Galdos, R., Vockel, M., Linnepe, R., Ipe, U., Stadtmann, A., Zarbock, A. et al. (2014). Leukocyte extravasation and vascular permeability are each controlled in vivo by different tyrosine residues of VE-cadherin. *Nat. Immunol.* **15**, 223-230. doi:10.1038/ni.2824

Yamamoto, H., Ehling, M., Kato, K., Kanai, K., van Lessen, M., Frye, M., Zeuschner, D., Nakayama, M., Vestweber, D. and Adams, R. H. (2015). Integrin β1 controls VE-cadherin localization and blood vessel stability. *Nat. Commun.* **6**, 6429. doi:10.1038/ncomms7429

Yue, J., Xie, M., Gou, X., Lee, P., Schneider, M. D. and Wu, X. (2014). Microtubules regulate focal adhesion dynamics through MAP4K4. *Dev. Cell* **31**, 572-585. doi:10.1016/j.devcel.2014.10.025